

CREDAL AND INTERVAL DEEP EVIDENTIAL CLASSIFICATIONS

BY MICHELE CAPRIO^{1,a}, SHIREEN K. MANCHINGAL^{2,b} AND FABIO CUZZOLIN^{2,c}

¹Department of Computer Science, The University of Manchester, ^amichele.caprio@manchester.ac.uk

²School of Engineering, Computing and Mathematics, Oxford Brookes University
^b19185895@brookes.ac.uk; ^cfabio.cuzzolin@brookes.ac.uk

Uncertainty Quantification (UQ) presents a pivotal challenge in the field of Artificial Intelligence (AI), profoundly impacting decision-making, risk assessment and model reliability. In this paper, we introduce Credal and Interval Deep Evidential Classifications (CDEC and IDEC, respectively) as novel approaches to address UQ in classification tasks. CDEC and IDEC leverage a credal set (closed and convex set of probabilities) and an interval of evidential predictive distributions, respectively, allowing us to avoid overfitting to the training data and to systematically assess both epistemic (reducible) and aleatoric (irreducible) uncertainties. When those surpass acceptable thresholds, CDEC and IDEC have the capability to abstain from classification and flag an excess of epistemic or aleatoric uncertainty, as relevant. Conversely, within acceptable uncertainty bounds, CDEC and IDEC provide a collection of labels with robust probabilistic guarantees. CDEC and IDEC are trained using standard backpropagation and a loss function that draws from the theory of evidence. They overcome the shortcomings of previous efforts, and extend the current evidential deep learning literature. Through extensive experiments on MNIST, CIFAR-10 and CIFAR-100, together with their natural OoD shifts (F-MNIST/K-MNIST, SVHN/Intel, TinyImageNet), we show that CDEC and IDEC achieve competitive predictive accuracy, state-of-the-art OoD detection under epistemic and total uncertainty, and tight, well-calibrated prediction regions that expand reliably under distribution shift. An ablation over ensemble size further demonstrates that CDEC attains stable uncertainty estimates with only a small ensemble.

1. Introduction. The notion of uncertainty has recently drawn increasing attention in machine learning (ML) and artificial intelligence (AI) due to the fields’ burgeoning relevance for practical applications (Sale, Caprio and Hüllermeier, 2023). Many such applications have safety requirements, such as medical domains (Lambrou, Papadopoulos and Gammernan, 2010; Senge et al., 2014; Yang et al., 2009) or socio-technical systems (Varshney, 2016; Varshney and Alemzadeh, 2017). These use cases in safety-critical contexts show that a suitable representation and quantification of uncertainty for modern, reliable machine learning systems is imperative.

In ML and AI, users are typically interested in two types of uncertainties, *aleatoric* and *epistemic* (AU and EU, respectively, formally introduced in section 3). The existing approaches to quantify AU and EU were extensively reviewed in (Hüllermeier and Waegeman, 2021).

Aleatoric uncertainty refers to the uncertainty that is inherent to the data generating process; as such, it is irreducible. Think, for example, of a coin toss. No matter how many times the coin is tossed, the stochastic variability of the experiment cannot be eliminated: we do not know with certainty what the outcome will be. Epistemic uncertainty, instead, refers to the lack of knowledge about the data generating process; as such, it is *reducible*. It can be

Keywords and phrases: Evidential deep learning, imprecise probabilities, credal sets, probability intervals, epistemic and aleatory uncertainties, uncertainty quantification, machine learning robustness.

lessened e.g. on the basis of additional data.¹ For example, after only a few tosses, we are unable to gauge whether a coin is biased or not, but if we repeat the experiment long enough, this type of uncertainty vanishes. In ML applications, EU can be typically reduced by retraining the model using an augmented training set (Lin et al., 2023) (e.g. via semantic preserving transformations (Kaur et al., 2023), Puzzle Mix (Kim, Choo and Song, 2020), etc.). On the other hand, since AU is irreducible, there is an increasing need for ML techniques that are able to detect an excess of AU and, in turn, flag such an excess and either abstain from producing a result, or warn to “proceed with caution”.

Distinguishing between AU and EU is then a crucial endeavor in (probabilistic) ML and AI. A single probability measure, though, can only capture aleatoric uncertainty, since it represents a case in which the agent knows the true data generating process precisely (Hüllermeier and Waegeman, 2021, Page 458). Because of that, researchers have proposed different deep learning techniques to disentangle AU and EU. Broadly, their efforts can be classified in the following four macro-categories (more related work can be found in Appendix B):

1. Methodologies based on Bayesian Deep Learning (Jospin et al., 2022; Kendall and Gal, 2017; Smith and Gal, 2018), such as Credal Bayesian Deep Learning (Caprio et al., 2024a). Although theoretically well-justified, they incur in large computational overheads, a consequence of the need to approximate the Bayesian posteriors (e.g. via variational inference).
2. Methodologies based on Dempster-Shafer theory, where uncertainty is modelled using random sets and fuzzy logic, such as Evidential Neural Networks (Denœux, 2000; Denœux, 2022, 2023; Denœux, Dubois and Prade, 2020; Denœux and Zouhal, 2001; Masson and Denœux, 2008) and Epistemic Deep Learning (Manchingal and Cuzzolin, 2022; Manchingal et al., 2023). These are theoretically well-justified and reasonably fast to implement. Nonetheless, they only focus on identifying and quantifying EU, and on taking the optimal decision as a consequence.
3. Methodologies based on second-order distributions (i.e., distributions over distributions), such as Kronecker-factored Quasi-Newton Methods (Ren, Bahamou and Goldfarb, 2022) and Evidential Deep Learning (EDL) (Ulmer, Hardmeier and Frelsen, 2023, and references therein). These have been recently shown to suffer from major pitfalls when used to quantify EU due to their sensitivity to regularization parameters, and to underestimate AU (Bengs, Hüllermeier and Waegeman, 2022; Jürgens et al., 2024; Pandey and Yu, 2023).
4. Ad-hoc methodologies, such as ensembles of neural networks (Egele et al., 2021). These are reasonably fast, but their measures of AU and EU are typically not theoretically well-justified. They are chosen for their intuitive appeal, or their ease of computation.

As we can see, all existing methodologies fall short of at least one of the following desirable properties: being (i) theoretically well-justified, (ii) fast to implement, (iii) able to properly quantify and disentangle both AU and EU. In response, we introduce two new deep learning techniques for classification problems that we call *Credal* and *Interval Deep Evidential Classifications* (CDEC and IDEC, respectively). They are EDL procedures that adopt a first-order distribution approach – so to overcome the shortcoming in (3) – and that build on concepts from Bayesian statistics, and the theories of credal sets and intervals of measures. Credal sets are closed and convex sets of probabilities (see also Definition 3.1), while intervals of measures are sets of probability density or mass functions that are derived by normalizing positive bounded measures (see also Definition 5.1). As we shall see in Proposition 5.2, credal sets and intervals of measures are related to each other. Once trained, given a new

¹EU should not be confused with *epistemic probability*, see Appendix A. It refers to the ignorance of the agent, and hence to the epistemic state of the agent instead of any underlying random phenomenon.

input \tilde{x} , CDEC produces a credal set of predictive distributions on the labels. Such credal set is used to gauge the uncertainty: if the total uncertainty (TU) is too high, CDEC abstains from producing a label for \tilde{x} and returns a warning for excess of AU or EU, as appropriate. If, instead, TU is not too high, it provides a collection of labels that contains the correct label for \tilde{x} with high probability. IDEC does the same, with an interval of predictive distributions in place of a credal set.

Notably, CDEC and IDEC address the three research challenges highlighted in (Ulmer, Hardmeier and Frellsen, 2023) as pivotal for EDL methods, as they: (i) allow an explicit estimation of EU and AU; (ii) are robust to model misspecification (via the predictive credal set/interval of measures); and (iii) give theoretical guarantees on the predicted label region. As Hüllermeier and Waegeman (2021) point out, measures of AU and EU based on credal sets are extremely well-justified from a theoretical point of view. CDEC and IDEC are also fast to implement, since they are based on backpropagation-trained neural networks.

We experimentally demonstrate the effectiveness of our approaches across several classification tasks. Firstly, we assess in-distribution predictive performance and show that our approaches improve accuracy and calibration across multiple datasets and backbones (Simple ConvNet, VGG16, ResNet18, ResNet50). Secondly, we show a marked improvement in out-of-distribution (OoD) detection, using several benchmark settings such as training on CIFAR-10 and evaluating on SVHN/Intel, MNIST on F-MNIST/K-MNIST, and CIFAR-100 on TinyImageNet. Additionally, we present results demonstrating the robustness of our classification sets and several ablation studies which provide deeper insights into the applicability of CDEC and IDEC. Specifically, the ablations reveal how epistemic uncertainty grows with ensemble diversity, and how CDEC maintains high coverage and consistent iD-OoD separation across ensemble sizes.

Contributions and structure of the paper. We introduce CDEC and IDEC, two deep learning techniques for classification that (i) are able to disentangle and quantify EU and AU in a theoretically sound manner, and to react appropriately to high levels of either (section 6.3); (ii) produce a label region with probabilistic guarantees (section 6.5); (iii) do not incur a large computational overhead, since CDEC requires only a small ensemble and IDEC operates with a single posterior model (section 6); and (iv) are empirically validated across predictive accuracy (section 6.2), uncertainty decomposition (section 6.3), OoD detection (section 6.4), and ensemble ablations (section 6.6).

The paper is divided as follows. Section 2 gives the necessary background to understand our results. Section 3 presents AU and EU in detail, and how to quantify them. Sections 4 and 5 introduces CDEC and IDEC, respectively. In section 6 we produce our experimental findings, and we conclude in section 7. We prove our results in Appendix G.

2. Background.

2.1. Dirichlet and Categorical Distributions. In this section, we introduce two distributions that are fundamental to understand the procedures presented in this paper (Hoff, 2009).

In a k -class classification problem, letting label Y_i be distributed according to a *Categorical distribution* is an extremely natural choice. In general, a Categorical $\text{Cat}(\pi)$ is parameterized by a k -dimensional probability vector π , that is, $\pi_j \geq 0$, for all $j \in \{1, \dots, k\}$, and $\sum_j \pi_j = 1$. Its probability mass function (pmf) is $P(\{j\}) \equiv p(Y_i = j) = \pi_j$, for all $j \in \{1, \dots, k\}$. That is, the probability of j being the “true label” is given by the j -th entry of vector π .

Adopting a Bayesian approach, we posit that π is itself a random quantity, and we need to elicit its distribution, that we call *prior*. Recall that the *conjugate prior* is the prior that, once combined with the likelihood, gives a posterior that belongs to the same family of

distributions, but with an updated parameter. Given our Categorical distribution $\text{Cat}(\pi)$, its conjugate prior is a *Dirichlet distribution* $\text{Dir}(\alpha)$. The latter is defined on the $(k - 1)$ -dimensional unit simplex, and it is parameterized by α , a k -dimensional vector whose entries are such that $\alpha_j \geq 1$, for all $j \in \{1, \dots, k\}$. Its probability density function (pdf) is given by $p(\pi) = 1/B(\alpha) \cdot \prod_{j=1}^k \pi_j^{\alpha_j-1}$, where $B(\cdot)$ denotes the multivariate Beta function. We can interpret the j -th entry of α as prior (or pseudo-) counts: α_j represents the (virtual) prior observations that we have for label j , and captures the agent’s prior knowledge around j (coming, for instance, from previous or similar experiments). The expected value of $\pi \sim \text{Dir}(\alpha)$ is given by $\mathbb{E}(\pi_j) = \alpha_j / \sum_{l=1}^k \alpha_l$, $j \in \{1, \dots, k\}$ (the normalised pseudo-count for class j), and expresses the prior belief that j is the “true” label.

Once combined with a $\text{Cat}(\pi)$ likelihood, the $\text{Dir}(\alpha)$ prior induces a $\text{Dir}(\alpha + c)$ posterior. Here, c is a k -dimensional vector whose j -th entry $c_j = n_j$ represents the number n_j of observations in the training set that are equal to j .

The corresponding (*posterior*) *predictive distribution*, that is, the probability distribution on the classes for a new (test) input \tilde{x} , is given by the Categorical distribution $\text{Cat}(\pi')$, where $\pi'_j = (\alpha_j + c_j) / \sum_{l=1}^k (\alpha_l + c_l)$, $j \in \{1, \dots, k\}$. It expresses the probability that the class \tilde{Y} for the new input \tilde{x} is equal to j , in light of what we learned from the data.

REMARK 1. *A Dirichlet distribution can be seen as a second-order distribution on the probabilities on $\{1, \dots, k\}$. To see this, notice that probability distributions with finite support can be written in the form of probability vectors. Suppose for example that $k = 3$, and that $P(\{1\}) = 0.6$, $P(\{2\}) = 0.3$, and $P(\{3\}) = 0.1$. Then, P is equivalent to the probability vector $(0.6, 0.3, 0.1)^\top$, which belongs to the 2-dimensional unit simplex. Hence, the $(k - 1)$ -unit simplex is equivalent to the class of all possible distributions supported on $\{1, \dots, k\}$. As a consequence, since Dirichlet distributions are supported on the unit simplex, they can be seen as distributions over distributions, or second-order distributions. EDL techniques typically take the second-order distribution approach when dealing with Dirichlet’s (Ulmer, Hardmeier and Frellsen, 2023), which leads to problems with the elicitation of EU (Bengs, Hüllermeier and Waegeman, 2022). To avoid these issues, in this paper we see Dirichlet’s as regular, first-order distributions.*

2.2. Posterior via Normalizing Flows. In this work, we use the EDL method proposed in Charpentier, Zügner and Günnemann (2020) to obtain the predictive distribution $\text{Cat}(\pi')$, which will be utilized in sections 4 and 5 to build a collection of labels that contains the correct one for a new input \tilde{x} with high probability. We opt for the technique in Charpentier, Zügner and Günnemann (2020) because, as pointed out by Ulmer, Hardmeier and Frellsen (2023), it provides the best result on the tested benchmarks, both in terms of task performance and uncertainty quality. This procedure is mainly concerned with deriving a “virtual” number n_j^{virt} of observations for category j , $j \in \{1, \dots, k\}$, by combining an encoder and a normalizing flow. We first illustrate the distributions involved, and then discuss how to derive n_j^{virt} , for all j .

Let $D = \{(x_i, y_i)\}_{i=1}^n$ be our training set, where, for all i , $x_i \in \mathcal{X}$ denotes an input and $y_i \in \mathcal{Y}$ is the output/label corresponding to x_i .² The values for n_j^{virt} are obtained as follows. We use the training set D to retrieve – via the loss in Charpentier, Zügner and Günnemann (2020, Equation (7)) – the parameters pair (θ, ϕ) , where the former parameterizes an encoder model f_θ that, once fed \tilde{x} , returns a latent representation $f_\theta(\tilde{x}) = \tilde{z}$ of input \tilde{x} . Then, a class-specific normalizing flow (Rezende and Mohamed, 2015) parameterized by ϕ assigns

²We denote by \mathcal{X} and \mathcal{Y} the input and output spaces, respectively.

a probability $q(\tilde{z} \mid y = j, \phi)$ to the latent representation \tilde{z} . In turn, $q(\tilde{z} \mid y = j, \phi)$ is used to weight the number n_j of observations in the training set D that are equal to j . In formulas,

$$n_j^{\text{virt}} = n_j \cdot q(\tilde{z} \mid y = j, \phi).$$

Call now $D^{\text{virt}} = \{(x_i, y_i)\}_{i=1}^{n^{\text{virt}}}$ our “virtual training set”, the training set in which the number of occurrences of label j is the value n_j^{virt} , as derived during training; in turn, $n^{\text{virt}} = \sum_{j=1}^k n_j^{\text{virt}}$. Notice that n^{virt} may well not be an integer. Writing $D = \{(x_i, y_i)\}_{i=1}^{n^{\text{virt}}}$ is a notational abuse that allows us to highlight the main feature of the method in [Charpentier, Zügner and Günnemann \(2020\)](#), that is, coming up with an evidential posterior predictive probability. We assume that there are $k = |\mathcal{Y}|$ classes. The procedure lets

$$(1) \quad \begin{aligned} Y_i \mid \pi, x_i &\sim \text{Cat}(\pi) \quad \text{i.i.d.}, \\ \pi &\sim \text{Dir}(\mathbf{1}_k), \end{aligned}$$

where $\mathbf{1}_k$ is a k -dimensional vector of all 1’s. Distribution $\text{Dir}(\mathbf{1}_k)$ is sometimes referred to as (k -dimensional) *Uniform Dirichlet*, and it captures the idea of agnostic prior beliefs.³ The posterior distribution of the classes, having observed the training data, is thus

$$\pi \mid D \sim \text{Dir}(\mathbf{1}_k + c),$$

where c is the vector of (virtual) counts introduced in section 2.1, that is, $c_j = n_j^{\text{virt}}$, for all j .

Given a new (test) input \tilde{x} , we get a predictive distribution of the form

$$\tilde{Y} \mid \tilde{x}, D \sim \text{Cat}(\pi'); \quad \pi'_j = \frac{1 + n_j^{\text{virt}}}{\sum_{l=1}^k (1 + n_l^{\text{virt}})}, \quad j \in \{1, \dots, k\}.$$

This procedure has the advantage of producing low probabilities for “strange” inputs, which in turn translate to low posterior counts $1 + n_j^{\text{virt}}$ of the Dirichlet posterior. This was used in [Charpentier, Zügner and Günnemann \(2020\)](#) to detect out-of-distribution (OoD) inputs.

3. Credal uncertainty modeling.

3.1. Likelihood Specification and Credal Sets. Let $p(y_i \mid \pi, x_i)$ denote the likelihood of the training pair (x_i, y_i) . Then, from our i.i.d. assumption in (1), the likelihood of the whole training set D is $\prod_{i=1}^{n^{\text{virt}}} p(y_i \mid \pi, x_i)$. This is again an abuse of notation since n^{virt} may well not be integer, and it means that the likelihood of D assigns a value of $\pi_j^{n_j^{\text{virt}}}$ to label j , for all $j \in \{1, \dots, k\}$.

As the values of the virtual number of observations n_j^{virt} ’s are a function of network parameters θ and ϕ (see section 2.2), different values of these parameters may result in (potentially noticeably) different likelihoods.⁴ How can we express, then, our uncertainty around which likelihood distribution is the “correct one”? That is, how can we hedge against likelihood misspecification? A natural idea – explored for the first time in the field of robust statistics in the 1970s ([Huber, 1973](#)) – is that of considering a set of “plausible” likelihoods ([Augustin et al., 2014](#); [Berger, 1984](#); [Caprio et al., 2024a](#); [Caprio and Mukherjee, 2023a](#); [Caprio et al., 2024b](#); [Caprio and Seidenfeld, 2023](#); [Gilboa et al., 2010](#); [Marinacci, 1999](#); [Walley, 1991](#)), or, more formally, a likelihood credal set.

³That is, at the beginning of the analysis we are either ignorant around which class is more likely to be the correct one, or indifferent among all the k classes, i.e. we believe they are all equally likely. Famously ([Walley, 1991](#)), a (precise) Uniform distribution cannot distinguish between these two cases. This is sometimes referred to as *Laplace’s paradox*.

⁴In practice, we vary θ and ϕ by varying the seeds of the encoder and of the normalized flow, respectively.

DEFINITION 3.1 (Credal Set (Levi, 1980)). A closed and convex set of probabilities \mathcal{P} is called a *credal set*.⁵ If a credal set \mathcal{P} has finitely many extreme elements, that is, if $|\text{ex}\mathcal{P}| < \infty$, it is called a *finitely generated credal set* (FGCS).

The extreme elements $P^{\text{ex}} \in \text{ex}\mathcal{P}$, or extrema, of a convex set are those that cannot be written as a convex combination of one another.

Consider $S \in \mathbb{N}_{\geq 2}$ many different encoders and normalized flows, whose respective outputs $f_{\theta_s}(\tilde{x}) = \tilde{z}_s$ and $q(\tilde{z}_s | y = j, \phi_s)$, $s \in \{1, \dots, S\}$,⁶ are used to elicit different values of the n_j^{virt} 's, which we denote by $n_{s,j}^{\text{virt}}$. Ultimately, this leads to specifying a finite set $\{\prod_{i=1}^{n_s^{\text{virt}}} p(y_i | \pi, x_i)\}_{s=1}^S$ of likelihoods of D , and, in turn, a likelihood FGCS

$$\mathcal{P}_{\text{lik}} = \text{Conv} \left(\left\{ \prod_{i=1}^{n_s^{\text{virt}}} p(y_i | \pi, x_i) \right\}_{s=1}^S \right),$$

where $\text{Conv}(\cdot)$ denotes the convex hull operator. That is, \mathcal{P}_{lik} is the set of all possible convex combinations of the elements of $\{\prod_{i=1}^{n_s^{\text{virt}}} p(y_i | \pi, x_i)\}_{s=1}^S$.⁷

We can then use the elements of $\{\prod_{i=1}^{n_s^{\text{virt}}} p(y_i | \pi, x_i)\}_{s=1}^S$ to derive a finite set $\{\text{Cat}(\pi'_s)\}_{s=1}^S$ of predictive Categorical distributions, where $\pi'_{s,j} = (1 + n_{s,j}^{\text{virt}}) / \sum_j (1 + n_{s,j}^{\text{virt}})$, for all $s \in \{1, \dots, S\}$ and all $j \in \{1, \dots, k\}$. By convex combination, this yields a predictive credal set

$$(2) \quad \mathcal{P}_{\text{pred}} = \text{Conv}(\{\text{Cat}(\pi'_s)\}_{s=1}^S).$$

As we can see, the uncertainty around the correct likelihood percolates through the classification procedure described in section 2.2, and manifests itself as predictive uncertainty encoded in (2). The assumption underlying the specification of \mathcal{P}_{lik} is that the “true” data generating process belongs to the likelihood FGCS \mathcal{P}_{lik} . Such an assumption can be tested via the techniques in Chau et al. (2025). If this holds, then the “true” predictive distribution belongs to the predictive FGCS $\mathcal{P}_{\text{pred}}$ derived from \mathcal{P}_{lik} .

Notice that, in general, the predictive FGCS $\mathcal{P}_{\text{pred}}$ can have less than S extreme elements. In formulas, $\text{ex}\mathcal{P}_{\text{pred}} \subseteq \{\text{Cat}(\pi'_s)\}_{s=1}^S$. This because it is possible that one or more of the S Categorical predictive distributions $\{\text{Cat}(\pi'_s)\}_{s=1}^S$ whose convex hull constitutes $\mathcal{P}_{\text{pred}}$ could be written as a convex combination of the other Categoricals. In Algorithm 1, Step 4, we give a way of precisely identifying the extreme elements $\text{ex}\mathcal{P}_{\text{pred}}$.

3.2. Aleatoric and Epistemic uncertainties. How can we distinguish between aleatoric and epistemic uncertainties in credal predictions of the form (2)?⁸ Recall that, given an arbitrary probability measure P on a finite (or countable) space \mathcal{Y} , its (Shannon) entropy is defined as $H(P) := -\sum_{y \in \mathcal{Y}} P(\{y\}) \log_2[P(\{y\})]$. For a (single) Categorical distribution $P_s = \text{Cat}(\pi'_s)$, this becomes

$$(3) \quad H(P_s) = -\sum_{j=1}^k \pi'_{s,j} \log_2(\pi'_{s,j}).$$

⁵Here closed has to be understood with respect to some topology endowed to the space of probabilities.

⁶Here we write $f_{\theta_s}(\tilde{x}) = \tilde{z}_s$ to highlight the fact that the value of \tilde{z}_s depends on the parameter θ_s , $s \in \{1, \dots, S\}$.

⁷Given its definition, the likelihood FGCS \mathcal{P}_{lik} can be seen as a *type-2 product* FGCS (Walley, 1991, Section 9.3).

⁸We are especially interested in predictive uncertainties, as our main focus is on the downstream performance of our approach.

The entropy primarily captures the shape of the pmf of P , namely its “peakedness” or non-uniformity (Dubois and Hüllermeier, 2007; Hüllermeier and Waegeman, 2021), and hence informs about the predictability of the outcome of a random experiment: the higher its value, the lower the predictability.

Consider instead an arbitrary credal set \mathcal{P} on \mathcal{Y} . Then, we can define the credal versions of the Shannon entropy as proposed by (Abellán, Klir and Moral, 2006; Hüllermeier and Waegeman, 2021), $\overline{H}(P) := \sup_{P \in \mathcal{P}} H(P)$ and $\underline{H}(P) := \inf_{P \in \mathcal{P}} H(P)$, called the *upper* and *lower (Shannon) entropy*, respectively. The upper entropy is a measure of total uncertainty, since it represents the minimum level of predictability associated with the elements of \mathcal{P} . In Abellán, Klir and Moral (2006); Hüllermeier and Waegeman (2021), the authors posit that it can be decomposed as a sum of aleatoric and epistemic uncertainties, and that the latter can be specified as the difference between upper and lower entropy, thus obtaining⁹

$$(4) \quad \underbrace{\overline{H}(P)}_{\text{total uncertainty TU}(\mathcal{P})} = \underbrace{\underline{H}(P)}_{\text{aleatoric uncertainty AU}(\mathcal{P})} + \underbrace{[\overline{H}(P) - \underline{H}(P)]}_{\text{epistemic uncertainty EU}(\mathcal{P})}.$$

We now give an “operative” upper bound to $\text{TU}(\mathcal{P}_{\text{pred}})$ in terms of the extreme elements $\text{ex}\mathcal{P}_{\text{pred}} \subseteq \{\text{Cat}(\pi'_s)\}_{s=1}^S$ of $\mathcal{P}_{\text{pred}}$.¹⁰ We also show that $\text{AU}(\mathcal{P}_{\text{pred}}) = \text{AU}(\text{ex}\mathcal{P}_{\text{pred}})$. These results are leveraged by our approach in Algorithm 1 (see section 4). In Appendix C, we also give a lower bound for $\text{EU}(\mathcal{P}_{\text{pred}})$, and both upper and lower bounds for $\text{EU}(\mathcal{P}_{\text{pred}})$.

THEOREM 3.2 (Total and Aleatoric Uncertainties). *Suppose, without loss of generality, that $\text{ex}\mathcal{P}_{\text{pred}} = \{\text{Cat}(\pi'_s)\}_{s=1}^S$. Let Δ^{S-1} denote the S -dimensional unit simplex,*

$$\Delta^{S-1} := \left\{ \beta = (\beta_1, \dots, \beta_S)^\top : \beta_s \geq 0 \text{ for all } s, \text{ and } \sum_s \beta_s = 1 \right\}.$$

Let $\underline{H}(P^{\text{ex}}) := \min_{P^{\text{ex}} \in \text{ex}\mathcal{P}_{\text{pred}}} H(P^{\text{ex}})$. Then,

$$(5) \quad \begin{aligned} \text{TU}(\mathcal{P}_{\text{pred}}) &= \overline{H}(P) \leq \sup_{\beta \in \Delta^{S-1}} \sum_{s=1}^S \beta_s H(P_s^{\text{ex}}) + \log_2(S) =: u[\text{TU}(\mathcal{P}_{\text{pred}})], \\ \text{AU}(\mathcal{P}_{\text{pred}}) &= \underline{H}(P) = \text{AU}(\text{ex}\mathcal{P}_{\text{pred}}) = \underline{H}(P^{\text{ex}}). \end{aligned}$$

Theorem 3.2 is extremely important, for it provides a simple way of calculating the AU and an easily computable upper bound for the TU of the predictive (finitely generated) credal set $\mathcal{P}_{\text{pred}}$. In particular, the entropy $H(P_s^{\text{ex}})$ of the extreme elements can be analytically computed as in (3), for all $s \in \{1, \dots, S\}$. Calculating $\underline{H}(P^{\text{ex}})$, then, is immediate. On the other hand, the quantity $\sup_{\beta \in \Delta^{S-1}} \sum_{s=1}^S \beta_s H(P_s^{\text{ex}})$ can be calculated in polynomial time.

We should note that upper and lower entropy are not the only tools for quantifying and disentangling AU and EU in the credal set framework. Other measures are also available (see (Bronevich and Rozenberg, 2021; Hofman, Sale and Hüllermeier, 2024; Chau, Caprio and Muandet, 2025), (Hüllermeier and Waegeman, 2021, Section 4.6.1) for a few examples) and they can be used in place of upper and lower entropy to quantify EU and AU within our predictive credal set $\mathcal{P}_{\text{pred}}$, as long as the measure chosen for the total uncertainty is bounded. In particular, we discuss about one such an alternative measure based on the generalized Hartley measure (GHM), together with the reason why we preferred upper and lower entropy (computing GHM being extremely costly even when $|\mathcal{Y}|$ is moderate), in Appendix D.

⁹For an exhaustive explanation of the validity of upper and lower entropy as uncertainty measures, we refer the interested reader to (Walley, 1991, Page 541) and (Augustin et al., 2014, Chapter 10.5.1).

¹⁰Here, by “operative” we mean that these bounds are easy to compute in practice.

4. Credal Deep Evidential Classification. In this section, we present our first procedure, that we call Credal Deep Evidential Classification (CDEC).

4.1. Imprecise Highest Density Regions. We first introduce the concepts of lower/upper probabilities and of $(1 - \gamma)$ -imprecise highest density region (IHDR).

DEFINITION 4.1 (Lower and Upper Probabilities). Let \mathcal{P} be a credal set on \mathcal{Y} . Then, its *lower envelope* $\underline{P}(A) = \inf_{P \in \mathcal{P}} P(A)$, for all $A \subseteq \mathcal{Y}$, is called the *lower probability* of \mathcal{P} . Its *upper envelope* $\overline{P}(A) = \sup_{P \in \mathcal{P}} P(A)$, for all $A \subseteq \mathcal{Y}$, is called the *upper probability* of \mathcal{P} .

Lower and upper probabilities are conjugate to each other, that is, $\overline{P}(A) = 1 - \underline{P}(A^c)$ and $\underline{P}(A) = 1 - \overline{P}(A^c)$, for all $A \subseteq \mathcal{Y}$, where $A^c := \mathcal{Y} \setminus A$. Hence, knowing one is sufficient to retrieve the other. The lower and upper probabilities of an FGCS \mathcal{P} coincide with those of the set of its extreme elements $\text{ex}\mathcal{P}$ (Dantzig, 1963), (Caprio et al., 2024a, Proposition 2).¹¹

DEFINITION 4.2 (Imprecise Highest Density Region (Coolen, 1992)). Let \mathcal{P} be a generic set of probabilities on a finite set \mathcal{Y} . Let \underline{P} be the lower probability of \mathcal{P} . Let Y be a random quantity that takes values in \mathcal{Y} . Let also γ be any value in $[0, 1]$. Then, set $IR_\gamma(\mathcal{P}) \subseteq \mathcal{Y}$ is called a $(1 - \gamma)$ -*Imprecise Highest Density Region* (IHDR) if $\underline{P}[Y \in IR_\gamma(\mathcal{P})] \geq 1 - \gamma$ and $|IR_\gamma(\mathcal{P})|$ is a minimum. The notation “IR” stands for “Imprecise Region”.

Let us give an example. Suppose $\mathcal{Y} = \{y_1, \dots, y_5\}$, $\text{ex}\mathcal{P} = \{P_1, P_2, P_3\}$, and $\gamma = 0.1$. The numerical values for $P(\{y_j\})$ are given in Table 1, for all $P \in \text{ex}\mathcal{P}$ and all $j \in \{1, \dots, 5\}$. Then, from Definition 4.2 and (Caprio et al., 2024a, Proposition 3), we have that $IR_\gamma(\mathcal{P}) = \{y_1, y_2, y_3\}$.

	y_1	y_2	y_3	y_4	y_5
P_1	0.7	0.25	0.03	0.01	0.01
P_2	0.6	0.2	0.1	0.05	0.05
P_3	0.5	0.3	0.15	0.025	0.025

TABLE 1

Numerical values for our example. It is easy to see that the smallest subset of \mathcal{Y} that is assigned a probability of at least 0.9 by all the elements of $\text{ex}\mathcal{P}$ is $\{y_1, y_2, y_3\}$.

By definition of lower probability, we know that $P[Y \in IR_\gamma(\mathcal{P})] \geq 1 - \gamma$, for all $P \in \mathcal{P}$; here lies the appeal of the IHDR concept. In this work, we are interested in the IHDR associated with $\mathcal{P}_{\text{pred}}$. Namely, $\mathcal{Y} = \{1, \dots, k\}$ is the list of classes/labels, and $IR_\gamma(\mathcal{P}_{\text{pred}})$ is the smallest collection of labels such that its lower probability is at least $1 - \gamma$, $\underline{P}[IR_\gamma(\mathcal{P}_{\text{pred}})] \geq 1 - \gamma$. An operative lower bound for $\underline{P}[IR_\gamma(\mathcal{P}_{\text{pred}})]$ can be given as follows.¹²

THEOREM 4.3 (Lower Bound for the Lower Probability of an IHDR). Let $IR_\gamma(\mathcal{P}_{\text{pred}})$ denote the $(1 - \gamma)$ -IHDR associated with $\mathcal{P}_{\text{pred}}$, for some $\gamma \in [0, 1]$. Then,

$$(6) \quad \underline{P}[IR_\gamma(\mathcal{P}_{\text{pred}})] \geq \sum_{y \in IR_\gamma(\mathcal{P}_{\text{pred}})} \underline{P}(\{y\}).$$

Notice that $\underline{P}(\{j\}) = \min_s \pi'_{s,j}$ thanks to (Caprio et al., 2024a, Proposition 2). This makes it easy to compute the bound in (6).

¹¹A version of (Caprio et al., 2024a, Proposition 2) for finitely additive probability measures can be found in (Walley, 1991, Section 3.6).

¹²As for Theorem 3.2, by “operative” we mean that this bound is easy to compute in practice.

4.2. *Credal Deep Evidential Classification.* Our first classification procedure is presented in Algorithm 1. We call it Credal Deep Evidential Classification because it is based on credal sets theory and – when TU is not too high – its output is an IHDR.

Algorithm 1 Credal Deep Evidential Classification (CDEC) – Training and Inference

During Training

Step 1 Specify S many random seeds for as many encoders and normalizing flows

Step 2 Obtain the S parameters pairs $\{(\theta_s, \phi_s)\}_{s=1}^S$ using the loss in (Charpentier, Zügner and Günnemann, 2020, Equation 7)

During Inference

Inputs: New input $\tilde{x} \in \mathcal{X}$

Parameters: Uncertainty threshold $\epsilon > 0$; Confidence parameter $\gamma \in [0, 1]$

Outputs: Abstain for excessive AU; Abstain for excessive EU; $(1 - \gamma)$ -IHDR $IR_\gamma(\mathcal{P}_{\text{pred}})$

Step 3 Derive π'_s as in section 2.2, for all $s \in \{1, \dots, S\}$

Step 4 Obtain the extreme elements $\text{ex}\mathcal{P}_{\text{pred}}$ of $\mathcal{P}_{\text{pred}} = \text{Conv}(\{\text{Cat}(\pi'_s)\}_{s=1}^S)$

Step 5 Compute and return $u[\text{TU}(\mathcal{P}_{\text{pred}})]$ and $\text{AU}(\mathcal{P}_{\text{pred}})$ using Theorem 3.2

Step 6

if $\log_2(k) - u[\text{TU}(\mathcal{P}_{\text{pred}})] \geq \epsilon$ **then**

 Compute and return the $(1 - \gamma)$ -IHDR $IR_\gamma(\mathcal{P}_{\text{pred}}) \subseteq \{1, \dots, k\}$

else if $\log_2(k) - u[\text{TU}(\mathcal{P}_{\text{pred}})] < \epsilon$ **and** $\text{AU}(\mathcal{P}_{\text{pred}})/u[\text{TU}(\mathcal{P}_{\text{pred}})] \geq 1/2$ **then**

 Abstain from producing an IHDR due to excess AU

else if $\log_2(k) - u[\text{TU}(\mathcal{P}_{\text{pred}})] < \epsilon$ **and** $\text{AU}(\mathcal{P}_{\text{pred}})/u[\text{TU}(\mathcal{P}_{\text{pred}})] < 1/2$ **then**

 Abstain from producing an IHDR due to excess EU

end if

During training, in Step 1, the designer selects a number S of random seeds for as many encoders and normalizing flows. Number S is linked to the ambiguity faced by the agent. The larger S – that is, the more random seed the agent specifies –, the higher the ambiguity.

In Step 2, the user obtains the S parameter pairs $\{(\theta_s, \phi_s)\}_{s=1}^S$ via the loss in Charpentier, Zügner and Günnemann (2020). During inference, a new input \tilde{x} is provided.

In Step 3, the designer derives parameters $\{\pi'_s\}_{s=1}^S$ for (posterior) predictive distributions $\{\text{Cat}(\pi'_s)\}_{s=1}^S$, as illustrated in section 2.2.

In Step 4, they obtain the elements of $\text{ex}\mathcal{P}_{\text{pred}}$. Notice that a convex mixture of Categorical distributions is again a Categorical. Hence, to obtain $\text{ex}\mathcal{P}_{\text{pred}}$ we must verify which elements of $\{\text{Cat}(\pi'_s)\}_{s=1}^S$ cannot be written as a convex combination of one another. This is done by running a convex hull algorithm like *gift wrapping* on $\{\pi'_s\}_{s=1}^S$ (Preparata and Shamos, 1985, Chapters 3, 4). We can do so because, for all s , distribution $\text{Cat}(\pi'_s)$ is uniquely identified by its parameter π'_s .

Step 5 computes $\text{AU}(\mathcal{P}_{\text{pred}})$ and the upper bound for $\text{TU}(\mathcal{P}_{\text{pred}})$ using Theorem 3.2.

As for Step 6, recall that $\log_2(k)$ is the highest possible entropy associated with a discrete distribution over k classes. By definition of upper entropy of a credal set, $\text{TU}(\mathcal{P}_{\text{pred}})$ is also bounded by $\log_2(k)$. Then, if $u[\text{TU}(\mathcal{P}_{\text{pred}})]$ is (too) close to $\log_2(k)$, for example if $\log_2(k) - u[\text{TU}(\mathcal{P}_{\text{pred}})] < \epsilon$, for some user-specified $\epsilon > 0$, then the total uncertainty is too high to allow for a prediction. In such a case, our procedure abstains. We distinguish whether this high uncertainty is aleatoric or epistemic in nature by checking if at least half of the total uncertainty is aleatoric.¹³ If that is the case, the algorithm reports an excess of AU. If the opposite is true, it reports an excess of EU. If, instead, the total uncertainty is not too high, our procedure returns the $(1 - \gamma)$ -IHDR for $\mathcal{P}_{\text{pred}}$, for some $\gamma \in [0, 1]$ of interest.

¹³To be more precise, if the predictive aleatoric uncertainty $\text{AU}(\mathcal{P}_{\text{pred}})$ accounts for at least half of the upper bound for the predictive TU, $u[\text{TU}(\mathcal{P}_{\text{pred}})]$.

REMARK 2. Notice that, given the value of $u[TU(\mathcal{P}_{pred})]$ in (5), the difference $\log_2(k) - u[TU(\mathcal{P}_{pred})]$ can only be larger than ϵ , for some $\epsilon > 0$, if the number of encoders and normalized flows does not exceed the number of labels, i.e. only if $S < k$. If $S \geq k$, instead, $u[TU(\mathcal{P}_{pred})] \geq \log_2(k)$, and we can conclude immediately that the total uncertainty is too high. The reason appears to be the following. The more uncertainty-averse the user is, the larger the value of S they will select, which is then translated by CDEC in a high value of TU associated with the credal set \mathcal{P}_{pred} . We also point out that this sensibility of the TU to the choice of S seems to relate the problem of selecting the “correct” value of S to the identifiability of the elements of a finite (ad)mixture model (Caprio and Mukherjee, 2023b, Theorem 2, Proposition 9). This will be further studied in future work. As we shall see in section 5, IDEC will provide an “optimal” choice S^* .

Notice that a $(1 - \gamma)$ -IHDR is intuitively similar to a $(1 - \gamma) \times 100\%$ confidence interval. Hence, standard choices for the value of γ are 0.1, 0.05, 0.01. Hyperparameter ϵ , instead, captures how dangerous it is to produce an output in the presence of high (total) uncertainty. In other words, it represents how safety-critical the application at hand is. The larger ϵ is, the more likely we are to abstain. In our experiments, we provide ablation studies for both γ and ϵ .

4.3. *Features of Credal Deep Evidential Classification.* To summarize, after training, given a new input \tilde{x} , our procedure

1. Is able to disentangle and quantify AU and EU, and to react appropriately to large values of both.
2. When the total uncertainty is not too large, it returns the smallest set that contains the correct label for \tilde{x} with probability (at least) $1 - \gamma$, where $\gamma \in [0, 1]$ is chosen by the user.

Furthermore, CDEC can be easily adapted to different EDL methods to obtain the posterior and the predictive distributions (e.g. the one developed in (Pandey and Yu, 2023), which overcomes one of the fundamental limitations of EDL methods, i.e. creating zero evidence regions, which prevent the model to learn from training samples falling into/near such regions), and to different measures of TU , AU , and EU , as long as the selected measure for TU is not unbounded.

We conclude with three comments. First, CDEC can be easily modified to produce just one class, instead of an IHDR. In Step 6 of Algorithm 1, if $\log_2(k) - u[TU(\mathcal{P}_{pred})] \geq \epsilon$, we can output the label having the highest lower probability. In formulas,

$$j^* \in \arg \max_{j \in \{1, \dots, k\}} \min \pi'_j,$$

where the minimum is taken over the parameters π' of the Categorical distributions in $\text{ex}\mathcal{P}_{pred} \subseteq \{\text{Cat}(\pi'_s)\}_{s=1}^S$, that is, the set of extreme elements of the predictive FGCS \mathcal{P}_{pred} .¹⁴ Intuitively, in this modified version, CDEC returns – when the total uncertainty is not too high – the least implausible class for the new input \tilde{x} , according to the combination of agnostic prior beliefs and available evidence (in the form of likelihood FGCS \mathcal{P}_{lik}). The price to pay is to forego control on the accuracy level $1 - \gamma$ of the class/label region produced by CDEC.

Second, Credal Deep Evidential Classification is heuristically similar to the Imprecise Dirichlet Model (IDM, (Bernard, 2005; Walley, 1996)) and to the Naive Credal Classifier

¹⁴Of course, the $\arg \max$ may not be a singleton. In that case, even this modified version would produce a set of classes/labels. This means that the least implausible class $j \in \{1, \dots, k\}$ for new input \tilde{x} is *likelihood-dependent*, that is, it changes under different values of the n_j^{virt} 's. If the designer is set on outputting just one class, then, they may select one element uniformly at random from the $\arg \max$.

(NCC, (Cozman, 2000; Zaffalon, 2002), (Augustin et al., 2014, Chapter 10)), but with two main differences: (i) we use Categorical instead of Multinomial likelihoods, and (ii) we account for possible likelihood misspecification via a credal set representation. That is, our method accrues to the study of imprecise sampling models, or “likelihood robustness” (Shyamkumar, 2000). Furthermore, while in the IDM a possible conflict between prior and data is not reflected by increased imprecision (Augustin et al., 2014, Chapter 7.4.3.3) – that is, IDM is not sensitive to the prior-data conflict – CDEC avoids this issue altogether, by considering a uniform Dirichlet prior, and a set of plausible likelihoods.

Finally, since CDEC produces class regions with a predefined level of accuracy $1 - \gamma$, it is also heuristically similar to Conformal Prediction (Shafer and Vovk, 2008). This latter, though, is a distribution-free method and hence it is not directly comparable to CDEC. An in-depth study of the relationship between model-based and model-free methods is out of the scope of the present paper, and will be inspected in future work.

5. Interval Deep Evidential Classification. In this section, we present a procedure – called Interval Deep Evidential Classification (IDEC) – that simplifies Algorithm 1. To do so, we use intervals of measures (Coolen, 1992; DeRoberts and Hartigan, 1981) instead of credal sets.

5.1. Intervals of Measures.

DEFINITION 5.1 (Interval of Measures). Let \mathcal{Y} be a set of interest. Let $\ell, u : \mathcal{Y} \rightarrow \mathbb{R}_+$ be two positive functionals on \mathcal{Y} . They are called *lower* and *upper measures*, respectively. Suppose that $0 \leq \ell(y) \leq u(y) < \infty$, for all $y \in \mathcal{Y}$. Then, the *interval of measures* $\mathcal{I}(\ell, u)$ is defined as

$$\mathcal{I}(\ell, u) := \left\{ g : \mathcal{Y} \rightarrow \mathbb{R}_+ \text{ s.t. } g(y) = \frac{h(y)}{\int_{\mathcal{Y}} h(y) dy}, \text{ with } \ell(y) \leq h(y) \leq u(y), \text{ for all } y \in \mathcal{Y} \right\}.$$

The functions ℓ and u are assumed continuous and such that $0 < \int_{\mathcal{Y}} \ell(y) dy \leq \int_{\mathcal{Y}} u(y) dy < \infty$.

Let us relate Definition 5.1 to our classification setting. Recall that $\mathcal{Y} = \{1, \dots, k\}$ denotes the set of labels. Throughout this section, we refer to the elements of \mathcal{Y} as y or j , interchangeably. Let ℓ be the pmf of predictive Categorical distribution $\text{Cat}(\pi')$. We also let $u(y) = (1 + d)\ell(y)$, for all $y \in \mathcal{Y}$ and some $d \geq 0$. Then, $\mathcal{I}(\ell, u)$ becomes the class of distributions on $\mathcal{Y} = \{1, \dots, k\}$ whose pmf evaluated at $y \in \mathcal{Y}$ is given by $g(y) = h(y) / \sum_{y \in \mathcal{Y}} h(y)$, and $h(y) \in [\ell(y), (1 + d)\ell(y)]$. By construction, the elements of $\mathcal{I}(\ell, (1 + d)\ell)$ are Categorical distributions.

EXAMPLE. Suppose that $\mathcal{Y} = \{1, 2, 3, 4\}$; let ℓ be the pmf of a Categorical with parameter $\pi' = (0.7, 0.2, 0.08, 0.02)^\top$, and pick $d = 1.58$. Then,

$$(7) \quad (1 + d)\ell(y) = \begin{cases} 1.806, & y = 1 \\ 0.516, & y = 2 \\ 0.2064, & y = 3 \\ 0.0516, & y = 4 \end{cases}.$$

This means that, for all $\mathfrak{h} \in \mathcal{I}(\ell, (1+d)\ell)$, we have

$$\mathfrak{h}(y) \in \begin{cases} [0.7, 1.806], & y = 1 \\ [0.2, 0.516], & y = 2 \\ [0.08, 0.2064], & y = 3 \\ [0.02, 0.0516], & y = 4 \end{cases}.$$

For example, we may have

$$\mathfrak{h}(y) = \begin{cases} 1.2, & y = 1 \\ 0.3, & y = 2 \\ 0.1, & y = 3 \\ 0.04, & y = 4 \end{cases},$$

and obtain a Categorical distribution with pmf

$$p(y) = \begin{cases} \frac{1.2}{1.2+0.3+0.1+0.04} \approx 0.7317, & y = 1 \\ \frac{0.3}{1.2+0.3+0.1+0.04} \approx 0.1829, & y = 2 \\ \frac{0.1}{1.2+0.3+0.1+0.04} \approx 0.061, & y = 3 \\ \frac{0.04}{1.2+0.3+0.1+0.04} \approx 0.0244, & y = 4 \end{cases}.$$

IDEC simplifies CDEC as follows. Instead of initializing S many different encoders and normalizing flows like we did in section 4, we only need one of each, so $S = 1$, and we can drop the s index.

Once obtained the parameters pair (θ, ϕ) using the loss in [Charpentier, Zügner and Günnemann \(2020, Equation 7\)](#), given a new input \tilde{x} we are able to derive the predictive parameter π' as explained in section 2.2. We let ℓ be the pmf of $\text{Cat}(\pi')$.

After that, we assume that the pmf $\hat{p}(y) \equiv p(\tilde{y} \mid \tilde{x}, D)$ of the “true” predictive distribution \hat{P} is such that $\hat{p} \in \mathcal{I}(\ell, (1+d)\ell)$, for some $d \geq 0$.¹⁵ In a sense, d accomplishes the same task as S in section 4. It captures the ambiguity faced by the designer: the larger d , the higher the ambiguity. We further explore this connection in Section 5.3. We now show that there exists a relationship between credal sets and intervals of measures.

PROPOSITION 5.2 (Linking Intervals of Measures with Credal Sets). *Given a generic interval $\mathcal{I}(\ell, u)$ of measures on \mathcal{Y} , we can always find a credal set \mathcal{P} on \mathcal{Y} that corresponds to $\mathcal{I}(\ell, u)$. Its lower and upper probabilities are given by*

$$\underline{P}(A) = \left(1 + \frac{\int_{A^c} u(y) dy}{\int_A \ell(y) dy}\right)^{-1} \quad \text{and} \quad \overline{P}(A) = \left(1 + \frac{\int_{A^c} \ell(y) dy}{\int_A u(y) dy}\right)^{-1}, \quad \text{for all } A \in \mathcal{A}_{\mathcal{Y}},$$

respectively, where $\mathcal{A}_{\mathcal{Y}}$ is the sigma-algebra endowed to \mathcal{Y} .

Proposition 5.2 was first proven in ([Walley, 1991, Section 4.6.4](#)); a consequence of Proposition 5.2 is that we can test our assumption that $\hat{p} \in \mathcal{I}(\ell, (1+d)\ell)$ by checking whether \hat{P} belongs to the credal set associated to $\mathcal{I}(\ell, (1+d)\ell)$ using the techniques in [Chau et al. \(2025\)](#).

¹⁵This assumption allows us to frame our model in the objective Bayes approach to probability ([Berger, 2004, 1984, 1990](#)). That is, positing that a “true” prior and a “true” likelihood exist, then we are able to derive the “true” posterior and, in turn, the “true” posterior predictive distribution \hat{P} .

In our classification setting, Proposition 5.2 tells us that, given an interval $\mathcal{I}(\ell, (1+d)\ell)$ of measures on $\mathcal{Y} = \{1, \dots, k\}$ for some $d \geq 0$, the following holds

(8)

$$\underline{P}(\{j\}) = \left(1 + \frac{(1+d) \sum_{y \in \mathcal{Y} \setminus \{j\}} \ell(y)}{\ell(j)}\right)^{-1} \quad \text{and} \quad \overline{P}(\{j\}) = \left(1 + \frac{\sum_{y \in \mathcal{Y} \setminus \{j\}} \ell(y)}{(1+d)\ell(j)}\right)^{-1},$$

for all $j \in \{1, \dots, k\}$. Also,

(9)

$$\underline{P}(A) = \left(1 + \frac{(1+d) \sum_{y \in A^c} \ell(y)}{\sum_{y \in A} \ell(y)}\right)^{-1} \quad \text{and} \quad \overline{P}(A) = \left(1 + \frac{\sum_{y \in A^c} \ell(y)}{(1+d) \sum_{y \in A} \ell(y)}\right)^{-1},$$

for all $A \subseteq \mathcal{Y}$. Let us give a simple example. Building on Example 5.1, let $\mathcal{I}(\ell, (1+d)\ell)$ be an interval of measures where ℓ is the pmf of $\text{Cat}(\pi' = (0.7, 0.2, 0.08, 0.02)^\top)$ and $d = 1.58$. Then, equation (8) – together with the definition of π' and (7) – tells us that a credal set \mathcal{P} corresponding to $\mathcal{I}(\ell, (1+d)\ell)$ is one whose lower and upper probabilities for the elements of \mathcal{Y} are given by

$$\underline{P}(\{y\}) = \begin{cases} (1 + \frac{0.516+0.2064+0.0516}{0.7})^{-1} \approx 0.4749, & y = 1, \\ (1 + \frac{1.806+0.2064+0.0516}{0.2})^{-1} \approx 0.0883, & y = 2, \\ (1 + \frac{1.806+0.516+0.0516}{0.08})^{-1} \approx 0.0326, & y = 3, \\ (1 + \frac{1.806+0.516+0.2064}{0.02})^{-1} \approx 0.0078, & y = 4 \end{cases}$$

and

$$\overline{P}(\{y\}) = \begin{cases} (1 + \frac{0.2+0.08+0.02}{1.806})^{-1} \approx 0.8575, & y = 1, \\ (1 + \frac{0.7+0.08+0.02}{0.516})^{-1} \approx 0.3921, & y = 2, \\ (1 + \frac{0.7+0.2+0.02}{0.2064})^{-1} \approx 0.1832, & y = 3, \\ (1 + \frac{0.7+0.2+0.08}{0.0516})^{-1} \approx 0.05, & y = 4 \end{cases},$$

respectively. We have the following important corollary.

COROLLARY 5.2.1 (Equivalence between Intervals of Measures and FGCSs). *Let \mathcal{Y} be a finite set. Then, given a generic interval $\mathcal{I}(\ell, (1+d)\ell)$ of measures on \mathcal{Y} for some $d \geq 0$, we can always find a finitely generated credal set \mathcal{P} on \mathcal{Y} that corresponds to $\mathcal{I}(\ell, (1+d)\ell)$. Its lower and upper probabilities are obtained as in (9), for all $A \subseteq \mathcal{Y}$.*

As pointed out in Section 5.1, in IDEC we let ℓ be the pmf of predictive distribution $\text{Cat}(\pi')$, and $u = (1+d)\ell$, for some $d \geq 0$. As a result of Corollary 5.2.1, there always exists a choice of S initial random seeds for CDEC that produces a predictive finitely generated credal set $\mathcal{P}_{\text{pred}}$ that corresponds to $\mathcal{I}(\ell, (1+d)\ell)$. Because of this, by implementing IDEC instead of CDEC, the user to foregoes the task of specifying S , an operation that can be challenging and be perceived as needing substantial expert knowledge. In addition, IDEC is faster to implement because it only requires to derive one Categorical predictive distribution. Furthermore, as we shall see in section 5.3, we are also able to find an optimal choice d^* for the value of $d \geq 0$.

5.2. Aleatoric and Epistemic Uncertainties in the Interval Setting. We now need to specify how do we quantify total, aleatoric, and epistemic uncertainties in $\mathcal{I}(\ell, (1+d)\ell)$, and how to compute the IHDR.

Let $\tilde{Y} \sim \text{Cat}(\pi')$.¹⁶ Following (Dubois and Hüllermeier, 2007; Hüllermeier and Waegeman, 2021), we posit that the TU can be decomposed as the sum of AU and EU, and we let

$$(10) \quad \underbrace{\mathbb{V}[(1+d)\tilde{Y}]}_{\text{TU}[\mathcal{I}(\ell, (1+d)\ell)]} = \underbrace{\mathbb{V}[\tilde{Y}]}_{\text{AU}[\mathcal{I}(\ell, (1+d)\ell)]} + \underbrace{(\mathbb{V}[(1+d)\tilde{Y}] - \mathbb{V}[\tilde{Y}])}_{\text{EU}[\mathcal{I}(\ell, (1+d)\ell_i)]}.$$

Here $\mathbb{V}[\cdot]$ denotes the variance operator. Notice also that $\mathbb{V}[(1+d)\tilde{Y}] = (1+d)^2\mathbb{V}[\tilde{Y}]$ and that $\mathbb{V}[(1+d)\tilde{Y}] - \mathbb{V}[\tilde{Y}] = (d^2 + 2d)\mathbb{V}[\tilde{Y}]$. By direct calculation, we have that

$$(11) \quad \mathbb{V}[\tilde{Y}] = \sum_{j=1}^k j^2 \pi'_j - \left(\sum_{j=1}^k j \pi'_j \right)^2.$$

Although we build on the decomposition in section 3, we use the variance instead of the entropy because $(1+d)\ell(\cdot)$ is a signed (positive) measure, but not a probability measure, and so its entropy is not well-suited to being an uncertainty measure. To see this, consider again the case of Example 5.1. There, we have that $H(\ell) = -\sum_{y=1}^4 \ell(y) \log_2(\ell(y)) \approx 1.23$, while $H[(1+d)\ell] = -\sum_{y=1}^4 [(1+d)\ell(y)] \log_2[(1+d)\ell(y)] \approx -0.36$. As we can see, although $(1+d)\ell(y) > \ell(y)$, for all $y \in \mathcal{Y}$, we have that $H(\ell) > H[(1+d)\ell]$.¹⁷ We defer to future work the study of the properties à la (Abellán and Klir, 2005; Hüllermeier and Waegeman, 2021; Jiroušek and Shenoy, 2018; Walley, 1991) of the terms in (10).

5.3. Prediction in the Interval Setting. We are left to compute the IHDR associated with $\mathcal{I}(\ell, (1+d)\ell)$. In (Coolen, 1992, Theorem 1 and Corollary 1), the author shows that the $(1-\gamma)$ -IHDR $IR_\gamma[\mathcal{I}(\ell, (1+d)\ell)]$ of the interval $\mathcal{I}(\ell, (1+d)\ell)$ of measures on \mathcal{Y} is equal to the $[1-\xi(d)]$ -highest density region $\mathcal{R}_{\xi(d)}$ of $\text{Cat}(\pi')$ (Hoff, 2009), where

$$\xi(d) = \gamma/[1 + (1-\gamma)d].$$

Similarly to Definition 4.2, we have that $\mathcal{R}_{\xi(d)} \subseteq \mathcal{Y}$ is the collection of labels such that $\Pr_{\tilde{Y} \sim \text{Cat}(\pi')}[\tilde{Y} \in \mathcal{R}_{\xi(d)}] \geq 1 - \xi(d)$, and $|\mathcal{R}_{\xi(d)}|$ is a minimum.

This means that $IR_\gamma[\mathcal{I}(\ell, (1+d)\ell)]$ is given by the smallest subset of $\mathcal{Y} = \{1, \dots, k\}$ (the set of classes) such that

$$(12) \quad \sum_{j \in IR_\gamma[\mathcal{I}(\ell, (1+d)\ell)]} \pi'_j \geq 1 - \frac{\gamma}{1 + (1-\gamma)d}.$$

This is immediately computable once we obtain π' . Let us pause here to add a discussion. First, notice that $\xi(d) \leq \gamma$, for all $d \geq 0$, and $\xi(d) = \gamma$ if and only if $d = 0$. This is an expected phenomenon: if the distribution was precise, our region IR_γ would actually guarantee a probabilistic coverage of $1 - \xi(d) \geq 1 - \gamma$. Second, there is a trade-off pertaining the choice

¹⁶As we saw in section 2.2, we should write $\tilde{Y} \mid \tilde{x}, D \sim \text{Cat}(\pi')$. In this section, we omit the conditioning part for notational clarity.

¹⁷In (Caprio et al., 2024a, Theorem 13), the authors introduce a way of computing the entropy $H(\underline{P})$ and $H(\overline{P})$ of the lower and of the upper probabilities \underline{P} and \overline{P} of a credal set, respectively. Then, they show that $H(\underline{P})$ is a lower bound for $\underline{H}(P)$ and that $H(\overline{P})$ is an upper bound for $\overline{H}(P)$. We defer to future work the use of $H(\underline{P})$ and $H(\overline{P})$ for \underline{P} and \overline{P} derived as in (8) and (9) to quantify TU, AU, and EU within interval of measures $\mathcal{I}(\ell, (1+d)\ell)$.

of d . Larger values will guarantee a higher coverage to IR_γ , but will also make the cardinality of IR_γ larger.

We now provide the optimal choice d^* for the value of d , that is, the one that minimizes the difference $(1 - \xi) - (1 - \gamma)$ that represents the *coverage discrepancy* between the precise distribution $\text{Cat}(\pi')$ and the interval of measures $\mathcal{I}(\ell, (1 + d)\ell)$. To find it, we proceed as follows. Compute the $(1 - \gamma)$ -highest density region \mathcal{R}_γ of $\text{Cat}(\pi')$. Put

$$(13) \quad \mathcal{R}_\gamma^* = \begin{cases} \mathcal{R}_\gamma & \text{if } \sum_{j \in \mathcal{R}_\gamma} \pi'_j > 1 - \gamma \\ \mathcal{R}_\gamma \cup \{\arg \max_{j \in \{1, \dots, k\} \setminus \mathcal{R}_\gamma} \pi'_j\} & \text{if } \sum_{j \in \mathcal{R}_\gamma} \pi'_j = 1 - \gamma \end{cases}.$$

Equation (13) means the following. In virtually all applications, the sum of the probabilities π'_j of the labels $j \in \mathcal{R}_\gamma$ will go above $1 - \gamma$. In that case, we let $\mathcal{R}_\gamma^* = \mathcal{R}_\gamma$. If instead the sum is exactly $1 - \gamma$, then region \mathcal{R}_γ^* includes all the labels in \mathcal{R}_γ plus the next most probable one. Next, compute the *actual coverage* $\sum_{j \in \mathcal{R}_\gamma^*} \pi'_j$ of \mathcal{R}_γ^* , set it equal to $(1 - \xi)$, and obtain the value of ξ . Of course, we will have $(1 - \xi) > (1 - \gamma)$. Finally, solve

$$(14) \quad \xi = \frac{\gamma}{1 + (1 - \gamma)d^*}.$$

Notice that now ξ and γ are fixed values, so this becomes an equation with only one unknown that can be solved analytically. Notice also that d^* is a function of γ , $d^* \equiv d^*(\gamma)$.

Let us give a simple example, connected to Example 5.1. Suppose that in the problem at hand we have $k = 4$ labels, so $\mathcal{Y} = \{1, 2, 3, 4\}$, and that $\pi' = (0.7, 0.2, 0.08, 0.02)^\top$. Then, suppose we are interested in a 95% coverage for our IHDR IR_γ , so we let $\gamma = 0.05$. We have $\mathcal{R}_{0.05}^* = \mathcal{R}_{0.05} = \{1, 2, 3\}$. Now, the actual coverage of $\mathcal{R}_{0.05}^*$ is given by $0.7 + 0.2 + 0.08 = 0.98$. Hence, we let $1 - \xi = 0.98$, that is, $\xi = 0.02$. Finally, we solve $0.02 = 0.05/[1 + 0.95d^*]$ to obtain $d^* \approx 1.58$.

Notice how, in light of Corollary 5.2.1, finding d^* is equivalent to a specific choice of the amount S^* of random seeds for as many encoders and normalizing flows – together with their values – in CDEC. In addition, by (13) and (14), d^* is the value that minimizes the coverage discrepancy between the precise and the imprecise models, for a given value of $\gamma \in [0, 1]$. In turn, this implies that IDEC can be seen as a case of CDEC where the choices of amount $S = S^*$ and numerical value of the random seeds used to derive predictive credal set $\mathcal{P}_{\text{pred}}$ are “optimal”. Here, optimality means that the choice of the amount S and numerical value of the random seeds used to derive predictive credal set $\mathcal{P}_{\text{pred}}$ is *informed by the* (imprecise probabilistic) $1 - \gamma$ *guarantee* that we want to achieve on the predictive label set.

5.4. Algorithm in the Interval Setting. We summarize IDEC in Algorithm 2. Recall that $\mathcal{Y} = \{1, \dots, k\}$ is the labels set of interest.

Notice that a random variable distributed according to a Categorical distribution has maximum variance when the latter is parameterized by $\frac{1}{k}$, that is, a k -dimensional vector whose entries are all $1/k$.¹⁸ Hence,

$$\mathbb{V}[(1 + d)\tilde{Y}] \leq \mathbb{V}[(1 + d)Y^{\max}] = (1 + d)^2 \mathbb{V}[Y^{\max}] = \frac{(1 + d)^2(k + 1)(k - 1)}{12},$$

for all $d \geq 0$, where $Y^{\max} \sim \text{Cat}(\frac{1}{k})$.¹⁹ As a consequence, if $\mathbb{V}[(1 + d)Y^{\max}] - \mathbb{V}[(1 + d)\tilde{Y}] < \epsilon$, for some $\epsilon > 0$, then the designer is facing high total uncertainty. In this situation, there

¹⁸Notice that such a distribution corresponds to a Discrete Uniform.

¹⁹We derived the value of $(1 + d)^2 \mathbb{V}[Y^{\max}]$ from (11) by putting $\pi'_j = 1/k$, for all $j \in \{1, \dots, k\}$.

Algorithm 2 Interval Deep Evidential Classification – Training and Inference

During Training

Step 1 Obtain the parameters pair (θ, ϕ) using the loss in (Charpentier, Zügner and Günnemann, 2020, Equation 7)

During Inference

Input: New input $\tilde{x} \in \mathcal{X}$

Parameters: Uncertainty threshold $\epsilon > 0$; Confidence parameter $\gamma \in [0, 1]$

Outputs: Abstain for excessive AU; Abstain for excessive EU; $(1 - \gamma)$ -IHDR

$IR_\gamma[\mathcal{I}(\ell, (1 + d^*)\ell)] = \mathcal{R}_{\xi(d^*)}$

Step 2 Derive π' as in section 2.2. Let ℓ be the pmf of $\text{Cat}(\pi')$

Step 3 Compute d^* according to (14), and assume $\hat{p} \in \mathcal{I}(\ell, (1 + d^*)\ell)$

Step 4 Compute $\mathbb{V}[(1 + d^*)\tilde{Y}]$ and $\mathbb{V}[(1 + d^*)Y^{\max}]$

Step 5

if $\mathbb{V}[(1 + d^*)Y^{\max}] - \mathbb{V}[(1 + d^*)\tilde{Y}] \geq \epsilon$ **then**

 Compute and return the $(1 - \gamma)$ -IHDR $IR_\gamma[\mathcal{I}(\ell, (1 + d^*)\ell)] = \mathcal{R}_{\xi(d^*)}$

else if $\mathbb{V}[(1 + d^*)Y^{\max}] - \mathbb{V}[(1 + d^*)\tilde{Y}] < \epsilon$ **and** $(1 + d^*)^{-2} \geq 1/2$ **then**

 Abstain from producing an IHDR due to excess AU

else if $\mathbb{V}[(1 + d^*)Y^{\max}] - \mathbb{V}[(1 + d^*)\tilde{Y}] < \epsilon$ **and** $(1 + d^*)^{-2} < 1/2$ **then**

 Abstain from producing an IHDR due to excess EU

end if

are two cases. Either the majority of the total uncertainty is aleatoric, or it is epistemic. We verify whether we are in either case, similarly to section 4.²⁰

Notice that $\mathbb{V}[\tilde{Y}]/\mathbb{V}[(1 + d^*)\tilde{Y}]$, that expresses the amount of AU relative to that of TU, is equal to $(1 + d^*)^{-2}$. If $(1 + d^*)^{-2} \geq 1/2$, then at least half of the total uncertainty is aleatoric in nature. Vice versa, if $(1 + d^*)^{-2} < 1/2$, then at least half of the total uncertainty is of epistemic type.

6. Experiments.

6.1. Implementation. In this section, we present an extensive empirical study of Credal Deep Evidential Classification (CDEC) and Interval Deep Evidential Classification (IDEC). Our experiments examine predictive performance, uncertainty quantification, abstention behavior, and out-of-distribution (OoD) robustness. We evaluate all methods across multiple datasets, architectures, and uncertainty-related tasks.

Datasets and preprocessing. We evaluate PostNet (Charpentier, Zügner and Günnemann, 2020), PostNet-3 (3 ensembles of PostNet), CDEC-3 (3 ensembles) and IDEC (single model) on standard multi-class image classification benchmarks: CIFAR-10 (Krizhevsky, Nair and Hinton, 2009), MNIST (LeCun and Cortes, 2005) and CIFAR-100 (Krizhevsky, 2012). These datasets allow us to evaluate our methods under both low-dimensional and high-dimensional visual variability. Each dataset is paired with naturally occurring out-of-distribution (OoD) shifts. For OoD detection, we use the following in-distribution (iD)/OoD pairings: CIFAR-10 vs SVHN (Netzer et al., 2011)/Intel-Image (Bansal, 2019), MNIST vs F-MNIST (Xiao, Rasul and Vollgraf, 2017)/K-MNIST (Clanuwat et al., 2018), and CIFAR-100 vs TinyImageNet (Le and Yang, 2015). All datasets are accessed through `torchvision` and uniformly processed through a backbone-aware pipeline. For convolutional architectures (‘conv’), MNIST images are normalized and kept at native resolution, while CIFAR datasets and OoD sets are resized to 32×32 . We apply only standard dataset normalization (dataset-specific mean/variance) and do not introduce augmentation, to avoid confounding uncertainty analyses.

²⁰ A subtle difference between the method in this section and the one in section 4 is discussed in Appendix E. There, we also give a way of quantifying the degree of conservativeness of $IR_\gamma[\mathcal{I}(\ell, (1 + d)\ell)]$.

Backbones and training details. We implement our method on four neural architectures: a lightweight convolutional network (‘conv’), VGG16, ResNet18, and ResNet50. The ‘conv’ architecture consists of three convolutional layers, each using 64 filters, LeakyReLU activations, and a kernel size of 5, with each layer followed by max-pooling with stride 2. All backbones are wrapped inside a Posterior Network, which produces Dirichlet evidence parameters and likelihood-flow induced virtual counts following the method of [Charpentier, Zügner and Günnemann \(2020\)](#). For each dataset-backbone pair we train models using ten different random seeds on NVIDIA A100 80GB GPUs, as detailed in Appendix I.1.

Each seed produces a distinct encoder and normalizing-flow configuration due to stochastic initialization, enabling the construction of credal sets and ensembles. Training is performed using the evidential loss of [Charpentier, Zügner and Günnemann \(2020\)](#). Network hyperparameters are fixed across all backbones: hidden layers of dimension [64,64,64], latent dimension 6, kernel dimension 5, and 6 radial-flow components. The networks are optimized using Adam with a fixed learning rate of 10^{-4} and a batch size of 128.

Hyperparameter settings. Across all experiments we employ a fixed confidence target of $1 - \gamma = 0.95$ for the computation of imprecise highest-density regions (IHDRs). IDEC uses this same γ to derive the optimal interval inflation parameter d^* , ensuring the imprecise prediction region achieves the desired coverage. In CDEC, the same confidence level determines whether the system abstains or issues a set-valued prediction. Training hyperparameters such as learning rates, latent-flow dimensions, and intermediate feature sizes (detailed in section I.1) are kept constant across all architectures to ensure comparability.

Experiments. Firstly, we evaluate in-distribution predictive performance across all datasets (MNIST, CIFAR-10, CIFAR-100) and all backbones (Conv, VGG16, ResNet18, ResNet50). For each method, PostNet, PostNet-3, CDEC-3 and IDEC, we report accuracy, Brier score, expected calibration error (ECE), and predictive confidence (Table 2, and full results in Tables 6–8). CDEC-3 uses the lower-envelope predictive distribution derived from extreme points of the credal set, while IDEC uses a single posterior together with its optimal interval inflation parameter d^* , ensuring the target IHDR coverage level.

Secondly, we analyze uncertainty decomposition into aleatoric (AU), epistemic (EU), and total uncertainty (TU) following the definitions in Equations (4) and (10). For CDEC-3, AU corresponds to the minimum entropy across extreme points of the credal set, and EU reflects entropy variation across these extremes. For IDEC, AU/EU/TU follow the interval-variance decomposition induced by d^* . We report the mean AU/EU/TU for all models in Table 2 and provide full uncertainty-density plots in Figures 4, 3, and 5. These KDEs show clear iD-OoD separation, especially for EU and TU.

Thirdly, we assess OoD robustness using AUROC and AUPRC for AU, EU, TU, and confidence (Algorithm H.2). We evaluate OoD shifts $\text{MNIST} \rightarrow \{\text{F-MNIST}, \text{K-MNIST}\}$, $\text{CIFAR-10} \rightarrow \{\text{SVHN}, \text{Intel}\}$, and $\text{CIFAR-100} \rightarrow \text{TinyImageNet}$. Representative results are reported in Table 2 and the full results across all backbones appear in Table 9. As validated in Appendix I.2.3, Figure 6 show that CDEC-3 produces the sharpest distinction between iD and OoD uncertainty, with IDEC showing a similar but weaker trend.

Fourthly, we analyze the structure of the learned credal sets through the Imprecise Highest Density Regions (IHDRs). Table 3 reports IHDR size and coverage across datasets and backbones, while Table 10 quantifies how IHDRs expand under distribution shift. Visualizations in Figure 1 and qualitative examples in Figure 8 reveal that CDEC-3 produces compact IHDRs on iD samples and systematically expands on OoD inputs, whereas IDEC forms larger and more variable IHDRs. Additional IHDR analysis is provided in Appendix I.2.4.

Finally, we conduct an ablation study on the effect of ensemble size for CDEC (section 6.6). Using ensembles of sizes $S \in \{1, 3, 5, 7, 10\}$, we compare IHDR size, coverage, and mean AU/EU/TU (Table 4) and visualize distributions in Figure 2. The results show

that CDEC stabilizes for $S \approx 3$, with larger ensembles increasing epistemic spread in a predictable, dataset-dependent manner.

Together, these evaluations provide a comprehensive empirical characterization of CDEC-3 and IDEC, demonstrating that both approaches achieve principled uncertainty quantification, robust abstention, and strong performance under distribution shift, while maintaining competitive predictive accuracy on the base classification task.

6.2. Predictive performance. In this section, we evaluate the in-distribution predictive behavior of PostNet, PostNet-3, CDEC-3 and IDEC across all datasets and backbones (see section 1.2.1). Predictive accuracy is computed in the standard way as the proportion of test samples for which the predicted class (the maximizer of the predictive mean of the Categorical distribution) coincides with the ground truth. Brier score is evaluated as the mean squared deviation between the predictive probability vector and the corresponding one-hot encoded target, thereby jointly capturing calibration and sharpness. Calibration quality is further quantified using the expected calibration error (ECE). For each method, predicted confidences are partitioned into fixed-width bins, and the absolute difference between the empirical accuracy and the mean confidence within each bin is weighted by the bin frequency and summed across all bins. The exact computation procedure is provided in Appendix H.1.

Dataset	Model	Prediction Performance			Uncertainty Estimation			OoD Detection Performance			
		Acc (%) (↑)	Brier (↓)	ECE (↓)	AU mean (↓)	EU mean (↓)	TU mean (↓)	AUROC (↑)	AUPRC (↑)	AUROC (↑)	AUPRC (↑)
MNIST	PostNet	92.24	0.0794	0.0102	2.3888	0.0000	2.3888	F-MNIST		K-MNIST	
	PostNet-3	99.04	0.0388	0.0311	0.3767	3.1372	3.5139	90.74	80.27	90.44	79.83
	CDEC-3	99.42	0.0914	0.0986	0.0033	1.3575	1.3608	95.12	93.47	95.59	94.58
	IDEC	99.31	0.0216	0.0054	0.0162	4.2985e15	4.2985e15	97.15	96.87	96.97	96.86
								96.61	92.63	93.85	90.40
CIFAR-10	PostNet	81.52	0.2868	0.0906	4.0245	0.0000	4.0245	SVHN		Intel	
	PostNet-3	84.12	0.1988	0.0369	3.2563	2.36	5.62	74.96	84.52	68.74	36.57
	CDEC-3	86.44	0.1180	0.1865	0.0776	1.6244	1.7019	75.17	83.66	73.60	38.69
	IDEC	82.88	0.2656	0.0805	0.1291	4.3278e16	4.3278e16	78.04	86.94	74.98	43.30
								75.04	84.41	70.17	36.52
CIFAR-100	PostNet	53.93	0.7281	0.2868	0.9391	0.0000	0.9391	TinyImageNet			
	PostNet-3	59.91	0.5182	0.0572	0.6989	1.7059	2.4048	AUROC(↑)		AUPRC(↑)	
	CDEC-3	62.84	0.4683	0.2618	0.1809	1.4482	1.6291	65.84		62.18	
	IDEC	58.29	0.6978	0.2595	0.2693	11203.7291	11203.9984	67.01		60.05	
								72.95		68.54	
							65.75		60.45		

TABLE 2

Full evaluation of predictive performance, uncertainty decomposition, and OoD detection for all models on MNIST, CIFAR-10, and CIFAR-100 using a ResNet-50 backbone. Results include accuracy, Brier score, ECE, mean AU/EU/TU, and EU-AUROC/AUPRC for the corresponding OoD datasets.

Table 2 reports predictive performance using a ResNet-50 backbone, while Tables 6, 7 and 8 in the Appendix 1.2.1 provide the full results for Conv, VGG16 and ResNet18. Across all settings, CDEC-3 consistently outperforms the baselines. On MNIST, CDEC-3 achieves the highest accuracy, while maintaining competitive calibration despite the extreme simplicity of the task. On CIFAR-10, CDEC-3 provides a clear improvement over both PostNet and PostNet-3. The trend persists on CIFAR-100, where the greater class complexity amplifies calibration errors in the baselines; here, CDEC-3 maintains the lowest Brier score and among the lowest ECE values across all backbones (see Appendix 1.2.1, Tables 6-8). This behavior is expected: CDEC-3 computes predictions from the *lower envelope* of a credal set, which corresponds to aggregating only the extreme (most informative) members of the Dirichlet ensemble. These extreme points typically exhibit low entropy and sharper class probabilities, leading to *more decisive predictions without overconfidence*. IDEC performs competitively in terms of point predictions, often matching PostNet-3 in accuracy and achieving some of the lowest ECE values on MNIST and CIFAR-10; however, the interval inflation required to

guarantee marginal coverage occasionally leads to flatter predictive distributions on CIFAR-100, which in turn increases the Brier score.

6.3. Uncertainty estimation. In addition to point predictions, we evaluate how each method decomposes predictive uncertainty into its aleatoric (AU), epistemic (EU), and total (TU) components. Table 2 reports the mean AU/EU/TU values under a ResNet-50 backbone, while the corresponding results for Conv, VGG16 and ResNet18 are provided in Appendix I.2.2 and Tables 6–8. We also provide in Appendix I.2.2 full uncertainty-density plots (Figures 4, 3, 5), showing the distribution of AU, EU and TU for in-distribution (in blue) and OoD samples.

Across all datasets and architectures, CDEC-3 produces the *sharpest and most informative* uncertainty profiles. Because CDEC-3 computes uncertainty from the extreme points of the credal set, AU corresponds to the minimum entropy across the most plausible predictive distributions, and EU corresponds to the entropy gap between extreme hypotheses. This naturally suppresses spurious epistemic mass and yields substantially lower TU than both PostNet and PostNet-3. The effect is particularly pronounced on CIFAR-100, where model misspecification is strongest and PostNet ensembles frequently inflate epistemic uncertainty.

IDEC exhibits a complementary behavior. Its variance-based epistemic inflation produces competitive AU and EU on simpler datasets (MNIST, CIFAR-10), but on CIFAR-100 the mandatory interval expansion needed to guarantee marginal coverage leads to excessively large epistemic terms (visible also in Figure 5), which dominate AU and consequently inflate TU. This matches the theoretical behavior expected from interval-based uncertainty: when predictive probability vectors are diffuse over many classes, even modest inflation parameters can magnify EU (see Equation (10)), resulting in very large TU values.

6.4. Out-of-distribution (OoD) detection. We next assess the ability of PostNet, PostNet-3, CDEC-3 and IDEC to distinguish in-distribution data from unseen OoD shifts. Following standard practice, we evaluate discrimination using AUROC and AUPRC (Algorithm H.2), applied to aleatoric (AU), epistemic (EU), total uncertainty (TU) and predictive confidence ('conf'). For confidence, higher values indicate more in-distribution behavior and are therefore negated before ranking. Table 2 reports the conf-based AUROC/AUPRC for ResNet-50 across all datasets, while the complete EU/AU/TU/conf based OoD detection results on all architectures are given in Appendix I.2.3 (Table 9).

Across all settings, CDEC-3 consistently yields the strongest OoD discrimination, particularly when ranking by epistemic or total uncertainty. This behavior follows directly from CDEC's credal construction: when an input drifts off the training manifold, the extreme points of the credal set diverge, amplifying epistemic spread and producing a clear separation between ID and OoD samples. IDEC also performs well on MNIST and CIFAR-10, though its required interval inflation occasionally leads to flatter predictive distributions on CIFAR-100, reducing contrast. A visual confirmation of this trend is provided in Appendix I.2.3, Figure 6, where we show KDEs of AU, EU and TU for CDEC-3 and IDEC on all datasets. In every case, the iD distribution is sharply concentrated, while OoD samples produce broader, right-shifted uncertainty profiles.

6.5. Imprecise Highest Density Region (IHDR) analysis. Table 3 summarizes the behavior of CDEC-3 and IDEC across datasets and backbones in terms of IHDR size and coverage. For all datasets, CDEC-3 produces *sharply concentrated* credal sets on iD data: IHDR sizes remain close to 1 on MNIST and below 7 on CIFAR-10, with perfect or near-perfect coverage across all backbones. In contrast, IDEC returns larger and more diffuse IHDRs, particularly on CIFAR-100, where its mean set size ranges from 36 to 61 depending on the backbone.

TABLE 3
IHDR set size and coverage for CDEC-3 and IDEC across datasets and backbones. Lower IHDR size and higher coverage is preferred.

Backbone	MNIST				CIFAR-10				CIFAR-100			
	CDEC-3		IDEC		CDEC-3		IDEC		CDEC-3		IDEC	
	Size	Cov	Size	Cov	Size	Cov	Size	Cov	Size	Cov	Size	Cov
Conv	1.3639	0.9994	6.3426	1.0000	6.8010	0.9975	6.7627	0.9966	98.8361	1.0000	43.9969	0.9644
VGG16	1.3780	0.9991	4.5456	1.0000	6.2122	0.9833	10.0000	1.0000	98.5251	1.0000	36.0142	0.8378
ResNet18	1.4473	0.9995	5.5165	0.9998	6.9749	0.9930	10.0000	1.0000	98.7851	0.9998	41.4300	0.9023
ResNet50	2.2789	0.9993	10.0000	1.0000	5.3438	0.9937	10.0000	1.0000	73.0291	0.9861	61.5121	0.9694

These results highlight a key structural difference: CDEC-3 encourages highly specific credal sets on iD inputs, whereas IDEC reflects more cautious and dispersed uncertainty.

Backbone choice primarily affects IDEC. Shallow architectures such as VGG amplify IDEC’s IHDR size (e.g. CIFAR-100 IHDR drops from 61.5 on ResNet50 to 36.0 on VGG), indicating that the learned credal structure is sensitive to representation quality. CDEC-3, on the other hand, is comparatively invariant to backbone variation: its IHDRs remain compact across Conv/VGG/ResNet, and its iD-OoD separation is preserved even when the backbone changes. The effect of distribution shift is examined in Table 10 in Appendix I.2.4, which compares mean IHDR size on iD inputs with the size obtained on one or more OoD datasets. For CDEC-3, IHDRs expand sharply under shift (by +3 to +7 on MNIST and CIFAR-10, and by +23 on CIFAR-100) yielding a strong and monotonic separation between iD and OoD. IDEC exhibits the same qualitative pattern on most settings, except that the magnitude of the expansion is smaller.

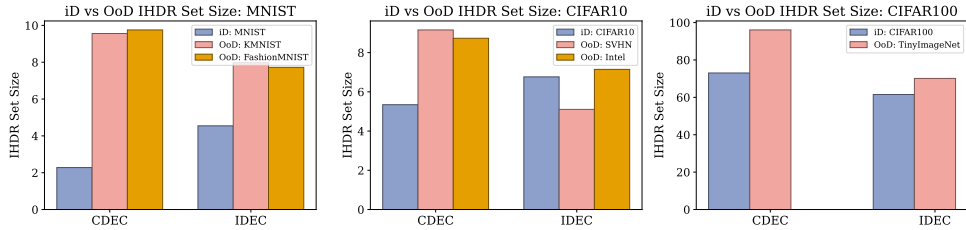


FIG 1. ***iD vs OoD IHDR set size across datasets.*** Bars show the mean IHDR cardinality for CDEC-3 and IDEC on in-distribution data (blue) and on one or two OoD datasets per benchmark (orange/salmon). CDEC-3 exhibits a clear expansion of the IHDR under distribution shift, whereas IDEC shows a smaller and less consistent separation between iD and OoD.

Figure 1 visualizes these trends. For each dataset, CDEC-3 yields small IHDRs on iD samples and large, clearly separated IHDRs on OoD inputs. IDEC shows a similar but less pronounced behavior: while its iD IHDRs are larger than those of CDEC-3, the contrast between iD and OoD is typically weaker. Overall, these results indicate that CDEC-3 provides the most consistent and interpretable behavior: it forms compact, well-calibrated credal sets on iD data while responding to distributional shift with a clear and systematic expansion in IHDR size.

In Appendix I.2.4, we show additional analysis on IHDR size, coverage and some qualitative illustrations of IHDRs (Figure 8) for randomly selected test samples of MNIST, CIFAR-10 and CIFAR-100 datasets.

6.6. The effect of ensemble numbers on CDEC. To study how the size of the CDEC ensemble influences the resulting credal sets and the decomposed uncertainties, we evaluate

CDEC with ensemble sizes $S \in \{1, 3, 5, 7, 10\}$ on MNIST, CIFAR-10, and CIFAR-100. Table 4 reports IHDR size, coverage, and the mean AU/EU/TU components for each setting, while Figure 2 visualizes the distribution of IHDR sizes together with coverage behavior.

TABLE 4

Ablation of CDEC ensemble size on IHDR quality and uncertainty across datasets. We report mean IHDR size (\downarrow), coverage (\uparrow), and mean AU/EU/TU (\downarrow) for ensemble sizes $S \in \{1, 3, 5, 7, 10\}$.

S	MNIST					CIFAR-10					CIFAR-100				
	IHDR(\downarrow)	Cov(\uparrow)	AU(\downarrow)	EU(\downarrow)	TU(\downarrow)	IHDR(\downarrow)	Cov(\uparrow)	AU(\downarrow)	EU(\downarrow)	TU(\downarrow)	IHDR(\downarrow)	Cov(\uparrow)	AU(\downarrow)	EU(\downarrow)	TU(\downarrow)
1	1.06	0.996	0.0264	0.0000	0.0264	2.30	0.949	0.4707	0.0000	0.4707	34.77	0.946	2.4064	0.0000	2.4064
3	1.36	0.999	0.0040	1.1469	1.1509	6.80	0.998	0.2165	1.6199	1.8364	98.84	1.000	1.7862	2.2833	4.0695
5	1.09	0.997	0.0288	0.4202	0.4490	2.13	0.944	0.4132	0.0000	0.4132	33.13	0.938	2.3321	0.0014	2.3335
7	1.36	0.999	0.0040	1.5301	1.5341	6.80	0.998	0.2165	2.4660	2.6825	98.72	1.000	1.7862	3.1269	4.9131
10	1.36	0.999	0.0040	1.9027	1.9067	6.80	0.998	0.2165	2.8227	3.0392	98.72	1.000	1.7862	3.4835	5.2697

IHDR size. Across all datasets, $S = 1$ (no ensembling) produces the smallest IHDR on MNIST, but the effect reverses on CIFAR-10 and CIFAR-100, where $S = 1$ yields substantially smaller (and in some cases underdispersed) credal sets compared to larger ensembles. For $S \geq 3$, the IHDR size stabilizes and becomes nearly invariant to S , indicating that CDEC’s epistemic decomposition quickly saturates with only a few ensemble members. On CIFAR-100, larger ensembles ($S \geq 3$) consistently produce substantially broader IHDRs, reflecting the increased epistemic ambiguity inherent in the dataset.

Coverage. Coverage remains close to 1 across all S on MNIST and CIFAR-100, confirming that CDEC maintains high reliability even as the ensemble grows. On CIFAR-10, coverage slightly drops for $S = 1$ and $S = 5$, but returns to near-perfect levels for $S \in \{3, 7, 10\}$. This suggests that moderate ensemble sizes mitigate instability in the epistemic component while preserving calibration.

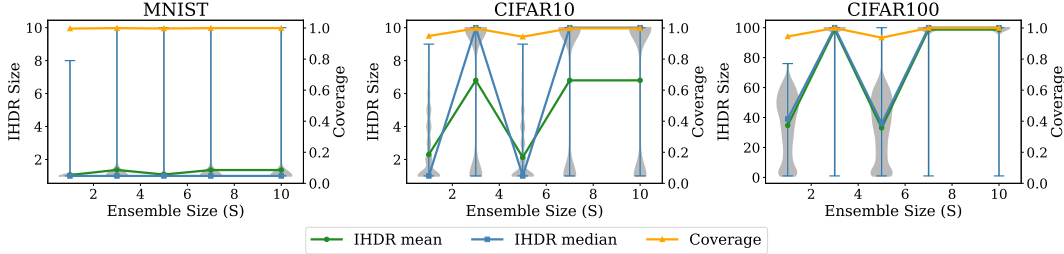


FIG 2. *Effect of ensemble size S on IHDR distributions and coverage for CDEC. IHDR sizes (violin + median) and coverage are shown for MNIST, CIFAR-10, and CIFAR-100. Ensemble sizes $S \geq 3$ yield stable IHDR behavior across datasets, whereas $S = 1$ underestimates epistemic uncertainty on CIFAR-10 and CIFAR-100.*

Uncertainty decomposition. The behavior of AU/EU/TU mirrors the IHDR trends. For $S = 1$, epistemic uncertainty (EU) is nearly zero on MNIST and CIFAR-10, as expected for a single posterior sample. As S increases, EU grows steadily and dominates TU, with AU remaining relatively stable. The increase in EU directly corresponds to the thickening of IHDR distributions in Figure 2 and reflects the epistemic diversity injected by the ensemble. On CIFAR-100, EU continues to grow with S , leading to a similarly increasing TU. This is consistent with the dataset’s higher class complexity and confirms that epistemic spread is the principal driver of IHDR expansion in CDEC.

Overall, the ablation reveals that: (i) CDEC requires only a small ensemble ($S \approx 3$) for stable IHDR behavior, (ii) larger ensembles produce wider IHDRs primarily through increased

epistemic uncertainty, and (iii) coverage remains near-perfect across datasets. These results demonstrate that CDEC’s decomposition behaves predictably with respect to ensemble size, and its epistemic component scales in a dataset-dependent way.

7. Conclusion. In this work, we introduced CDEC and IDEC, two evidential deep learning techniques that are able to gauge AU and EU in a classification problem; this is useful in abstaining from producing an output when excessive uncertainty is detected. The theoretical framework is grounded in the theories of credal sets and intervals of measures. We also showed their competitive performance via extensive experiments.

Throughout the paper, we assumed that the number of labels is known. In the future, we will forego this assumption. A high-level idea of how to proceed in that case is presented in Appendix F.

In addition, we plan to extend CDEC and IDEC to be able to deal with regression problems as well. This seems to be a difficult endeavor, as the one-to-one relationship between a Categorical distribution and its parameter that we exploited in Step 4 of Algorithm 1 may not hold in general (Jürgens et al., 2024, Theorem 3).

Furthermore, we aim at improving the elicitation process of the likelihood FGCS \mathcal{P}_{lik} for CDEC. There are two ways of achieving this goal. First, we could adopt a profile likelihood approach (Pawitan, 2001). After having specified our finite collection of likelihoods $\{\prod_{i=1}^{n_s^{\text{virt}}} p(y_i | \pi, x_i)\}_{s=1}^S$, we would compute the *normalized likelihood*

$$\text{lik}_s := \frac{\prod_{i=1}^{n_s^{\text{virt}}} p(y_i | \pi, x_i)}{\sup_{\pi \in \Delta^{k-1}} \prod_{i=1}^{n_s^{\text{virt}}} p(y_i | \pi, x_i)}, \quad s \in \{1, \dots, S\},$$

where Δ^{k-1} denotes the $(k-1)$ -dimensional unit simplex. At this point, we would remove from our collection $\{\prod_{i=1}^{n_s^{\text{virt}}} p(y_i | \pi, x_i)\}_{s=1}^S$ the likelihoods whose profile likelihood is below a threshold $\varphi \in [0, 1]$, thus obtaining

$$\mathcal{P}_{\text{lik}} = \text{Conv} \left(\left\{ \prod_{i=1}^{n_s^{\text{virt}}} p(y_i | \pi, x_i) : \text{lik}_s \geq \varphi, s \in \{1, \dots, S\} \right\} \right).$$

Standard values for φ are 0.75 and 0.95 (Antonucci, Cattaneo and Corani, 2011). A second way would be that of using a Large Language Model (LLM, (Brown et al., 2020)) to elicit a credal set starting from some qualitatively assessments of the data generating process. Upon receiving a prompt that contains information expressed in natural language, the LLM should output a finite collection of distributions, whose convex hull would constitute the likelihood FGCS \mathcal{P}_{lik} . For example, upon receiving a prompt containing a sentence like “I believe the data come from a distribution whose representation is some regularly looking, symmetric, bell-shaped curve”, the LLM should output a few Normals, Cauchy’s, and t-distributions. In the presence of a sentence like “My degree of uncertainty is high”, such distributions should be far from each other, e.g. in the total variation distance.

Finally, we intend to let go of the assumption in (1) that, conditional on π and x_i , the Y_i ’s are i.i.d. In future work, we will inspect the case where the Y_i ’s are identically distributed, but potentially dependent. A possible way of achieving this goal is to design a procedure that draws on the Lazy Naive Credal Classifier (LNCC, (Corani and Zaffalon, 2009), (Augustin et al., 2014, Chapter 10.4.1)). Such a method would go as follows. We would defer the training until a new input \tilde{x} has to be classified. Then, we would select m inputs $\{x_i\}_{i=1}^m$ from the training set that are close to \tilde{x} . In formulas, $\{x_i\}_{i=1}^m$, $m \leq n$, such that $d_{\mathcal{X}}(x_i, \tilde{x}) \leq \eta$, for some $\eta > 0$ and some metric $d_{\mathcal{X}}$ on the input space \mathcal{X} . After that, we would train our model on the restricted dataset $D^{\tilde{x}} := \{(x_i, y_i)\}_{i=1}^m$ formed by the inputs x_i that are closest to \tilde{x} and

their corresponding outputs y_i . Finally, we would only keep in memory the whole dataset $\{(x_i, y_i)\}_{i=1}^n$, and discard the locally trained classifiers. This way of proceeding, that works locally, reduces the chance of encountering strong dependencies between the classes (Frank, Hall and Pfahringer, 2002). The “right” value of η could be chosen empirically, e.g. by cross-validation on the training set, or by tuning it separately for each new input \tilde{x} (Corani and Zaffalon, 2009). Another way of letting go of assumption (1) is to explicitly model the dependencies between the elements of the dataset. This can be achieved e.g. via a decision tree, as done in Tree-Based Credal Classifiers (TBCCs, (Zaffalon and Fagioli, 2003), (Augustin et al., 2014, Chapter 10.5)).

Acknowledgments. The authors would like to thank Kuk Jin Jang, Yusuf Sale, and Malena Español for their helpful comments that helped shaping up the final version of the paper.

Funding. The first author was supported by ARO Grant ARO-MURI W911NF2010080.

REFERENCES

- ABELLÁN, J. and KLIR, G. J. (2005). Additivity of uncertainty measures on credal sets. *International Journal of General Systems* **34** 691–713.
- ABELLÁN, J., KLIR, G. J. and MORAL, S. (2006). Disaggregated total uncertainty measure for credal sets. *International Journal of General Systems* **1** 29–44.
- ANTONUCCI, A., CATTANEO, M. E. G. V. and CORANI, G. (2011). Likelihood-Based Naive Credal Classifier. In *ISIPTA '11, Proceedings of the Seventh International Symposium on Imprecise Probability: Theories and Applications* (F. P. A. COOLEN, G. DE COOMAN, T. FETZ and M. OBERGUGGENBERGER, eds.) 21–30. SIPTA.
- AUGUSTIN, T., COOLEN, F. P. A., DE COOMAN, G. and TROFFAES, M. C. M., eds. (2014). *Introduction to imprecise probabilities*. Wiley Series in Probability and Statistics. John Wiley and Sons.
- BANSAL, P. (2019). Intel image classification. Available on <https://www.kaggle.com/puneet6060/intel-image-classification>, Online.
- BENGS, V., HÜLLERMEIER, E. and WAEGEMAN, W. (2022). Pitfalls of Epistemic Uncertainty Quantification through Loss Minimisation. In *Advances in Neural Information Processing Systems* (S. KOYEJO, S. MOHAMED, A. AGARWAL, D. BELGRAVE, K. CHO and A. OH, eds.) **35** 29205–29216. Curran Associates, Inc.
- BERGER, J. O. (1984). The robust Bayesian viewpoint. In *Robustness of Bayesian Analyses* (J. B. Kadane, ed.) Amsterdam : North-Holland.
- BERGER, J. O. (1990). Robust Bayesian analysis: sensitivity to the prior. *Journal of Statistical Planning and Inference* **25** 303–328.
- BERGER, J. (2004). The case for objective Bayesian analysis. *Bayesian Analysis* **1** 1–17.
- BERNARD, J.-M. (2005). An introduction to the imprecise Dirichlet model for multinomial data. *International Journal of Approximate Reasoning* **39** 123–150. Imprecise Probabilities and Their Applications.
- BRONEVICH, A. G. and ROZENBERG, I. N. (2021). Generalized Hartley Measures on Credal Sets. In *Proceedings of the Twelfth International Symposium on Imprecise Probability: Theories and Applications* (A. CANO, J. DE BOCK, E. MIRANDA and S. MORAL, eds.). *Proceedings of Machine Learning Research* **147** 32–41. PMLR.
- BROWN, T., MANN, B., RYDER, N., SUBBIAH, M., KAPLAN, J. D., DHARIWAL, P., NEELAKANTAN, A., SHYAM, P., SASTRY, G., ASKELL, A., AGARWAL, S., HERBERT-VOSS, A., KRUEGER, G., HENIGHAN, T., CHILD, R., RAMESH, A., ZIEGLER, D., WU, J., WINTER, C., HESSE, C., CHEN, M., SIGLER, E., LITWIN, M., GRAY, S., CHESS, B., CLARK, J., BERNER, C., MCCANDLISH, S., RADFORD, A., SUTSKEVER, I. and AMODEI, D. (2020). Language Models are Few-Shot Learners. In *Advances in Neural Information Processing Systems* (H. LAROCHELLE, M. RANZATO, R. HADSELL, M. F. BALCAN and H. LIN, eds.) **33** 1877–1901. Curran Associates, Inc.
- CAPRIO, M. and MUKHERJEE, S. (2023a). Ergodic theorems for dynamic imprecise probability kinematics. *International Journal of Approximate Reasoning* **152** 325–343. <https://doi.org/10.1016/j.ijar.2022.10.016>
- CAPRIO, M. and MUKHERJEE, S. (2023b). Finite admixture models: a bridge with stochastic geometry and Choquet theory. Available at [arXiv:2002.08409](https://arxiv.org/abs/2002.08409).
- CAPRIO, M. and SEIDENFELD, T. (2023). Constriction for sets of probabilities. In *Proceedings of the Thirteenth International Symposium on Imprecise Probability: Theories and Applications* (E. MIRANDA, I. MONTES, E. QUAEGHEBEUR and B. VANTAGGI, eds.). *Proceedings of Machine Learning Research* **215** 84–95. PMLR.

- CAPRIO, M., DUTTA, S., JANG, K. J., LIN, V., IVANOV, R., SOKOLSKY, O. and LEE, I. (2024a). Credal Bayesian Deep Learning. *Transactions on Machine Learning Research*.
- CAPRIO, M., SALE, Y., HÜLLERMEIER, E. and LEE, I. (2024b). A Novel Bayes' Theorem for Upper Probabilities. In *Epistemic Uncertainty in Artificial Intelligence* (F. CUZZOLIN and M. SULTANA, eds.) 1–12. Springer Nature Switzerland, Cham.
- CERREIA-VIOGLIO, S., MACCHERONI, F. and MARINACCI, M. (2015). Ergodic theorems for lower probabilities. *Proceedings of the American Mathematical Society* **144** 3381–3396.
- CHARPENTIER, B., ZÜGNER, D. and GÜNNEMANN, S. (2020). Posterior Network: Uncertainty Estimation without OOD Samples via Density-Based Pseudo-Counts. In *Advances in Neural Information Processing Systems* (H. LAROCHELLE, M. RANZATO, R. HADSELL, M. F. BALCAN and H. LIN, eds.) **33** 1356–1367. Curran Associates, Inc.
- CHAU, S. L., CAPRIO, M. and MUANDET, K. (2025). Integral Imprecise Probability Metrics.
- CHAU, S. L., SCHRAB, A., GRETTON, A., SEJDINOVIC, D. and MUANDET, K. (2025). Credal Two-Sample Tests of Epistemic Uncertainty. In *Proceedings of The 28th International Conference on Artificial Intelligence and Statistics* (Y. LI, S. MANDT, S. AGRAWAL and E. KHAN, eds.). *Proceedings of Machine Learning Research* **258** 127–135. PMLR.
- CHICKERING, D. M., HECKERMAN, D. and MEEK, C. (2004). Large-Sample Learning of Bayesian Networks is NP-Hard. *The Journal of Machine Learning Research* **5** 1287–1330.
- CLANUWAT, T., BOBER-IRIZAR, M., KITAMOTO, A., LAMB, A., YAMAMOTO, K. and HA, D. (2018). Deep learning for classical Japanese literature. *arXiv preprint arXiv:1812.01718*.
- COOLEN, F. P. A. (1992). Imprecise highest density regions related to intervals of measures. *Memorandum COSOR* **9254**.
- CORANI, G., ANTONUCCI, A. and ZAFFALON, M. (2012). *Bayesian Networks with Imprecise Probabilities: Theory and Application to Classification* 4 of Data Mining: Foundations and Intelligent Paradigms: Volume 1: Clustering, Association and Classification, 49–93. Berlin, Germany : Springer.
- CORANI, G. and ZAFFALON, M. (2009). Lazy Naive Credal Classifier. In *Proceedings of the 1st ACM SIGKDD Workshop on Knowledge Discovery from Uncertain Data. U '09* 30–37. Association for Computing Machinery, New York, NY, USA. <https://doi.org/10.1145/1610555.1610560>
- COZMAN, F. G. (2000). Credal networks. *Artificial Intelligence* **120** 199–233. [https://doi.org/10.1016/S0004-3702\(00\)00029-1](https://doi.org/10.1016/S0004-3702(00)00029-1)
- DANTZIG, G. B. (1963). *Linear Programming and Extensions*. Princeton University Press.
- DE FINETTI, B. (1974). *Theory of Probability* **1**. New York : Wiley.
- DE FINETTI, B. (1975). *Theory of Probability* **2**. New York : Wiley.
- DENOËUX, T. (2000). A neural network classifier based on Dempster-Shafer theory. *IEEE Transactions on Systems, Man, and Cybernetics - Part A: Systems and Humans* **30** 131–150. <https://doi.org/10.1109/3468.833094>
- DENOËUX, T. (2022). An Evidential Neural Network Model for Regression Based on Random Fuzzy Numbers. In *Belief Functions: Theory and Applications* (S. LE HÉGARAT-MASCLE, I. BLOCH and E. ALDEA, eds.) 57–66. Springer International Publishing, Cham.
- DENOËUX, T. (2023). Quantifying Prediction Uncertainty in Regression using Random Fuzzy Sets: the ENNreg model. *IEEE Transactions on Fuzzy Systems* 1–10.
- DENOËUX, T., DUBOIS, D. and PRADE, H. (2020). Representations of Uncertainty in AI: Beyond Probability and Possibility. In *A Guided Tour of Artificial Intelligence Research: Volume I: Knowledge Representation, Reasoning and Learning* 119–150. Springer International Publishing, Cham.
- DENOËUX, T. and ZOUHAL, L. M. (2001). Handling possibilistic labels in pattern classification using evidential reasoning. *Fuzzy Sets and Systems* **122** 409–424.
- DEROBERTS, L. and HARTIGAN, J. A. (1981). Bayesian Inference Using Intervals of Measures. *The Annals of Statistics* **9** 235 – 244.
- DUBOIS, D. and HÜLLERMEIER, E. (2007). Comparing probability measures using possibility theory: A notion of relative peakedness. *International Journal of Approximate Reasoning* **45** 364–385. Eighth European Conference on Symbolic and Quantitative Approaches to Reasoning with Uncertainty (ECSQARU 2005).
- EGELE, R., MAULIK, R., RAGHAVAN, K., BALAPRAKASH, P. and LUSCH, B. (2021). AutoDEUQ: Automated Deep Ensemble with Uncertainty Quantification. *CoRR* **abs/2110.13511**.
- FRANK, E., HALL, M. and PFAHRINGER, B. (2002). Locally Weighted Naive Bayes. In *Proceedings of the Nineteenth Conference on Uncertainty in Artificial Intelligence. UAI'03* 249–256. Morgan Kaufmann Publishers Inc., San Francisco, CA, USA.
- FRÜHWIRTH-SCHNATTER, S., MALSINER-WALLI, G. and GRÜN, B. (2021). Generalized Mixtures of Finite Mixtures and Telescoping Sampling. *Bayesian analysis* **16** 1279–1307.
- GILBOA, I., MACCHERONI, F., MARINACCI, M. and SCHMEIDLER, D. (2010). Objective and subjective rationality in a multiple prior model. *Econometrica* **78** 755–770.

- HILL, B. M. (1968). Posterior Distribution of Percentiles: Bayes' Theorem for Sampling from a Population. *Journal of the American Statistical Association* **63** 677–691.
- HOFF, P. D. (2009). *A First Course in Bayesian Statistical Methods*. New York : Springer.
- HOFMAN, P., SALE, Y. and HÜLLERMEIER, E. (2024). Quantifying Aleatoric and Epistemic Uncertainty: A Credal Approach. In *ICML 2024 Workshop on Structured Probabilistic Inference & Generative Modeling*.
- HUBER, P. J. (1973). The use of Choquet capacities in statistics. *Bulletin of the International Statistical Institute* **45** 181–191.
- HÜLLERMEIER, E. and WAEGEMAN, W. (2021). Aleatoric and epistemic uncertainty in machine learning: an introduction to concepts and methods. *Machine Learning* **3** 457–506.
- JIROUŠEK, R. and SHENOY, P. P. (2018). A new definition of entropy of belief functions in the Dempster–Shafer theory. *International Journal of Approximate Reasoning* **92** 49–65.
- JOSPIN, L. V., LAGA, H., BOUSSAID, F., BUNTINE, W. and BENNAMOUN, M. (2022). Hands-On Bayesian Neural Networks – A Tutorial for Deep Learning Users. *IEEE Computational Intelligence Magazine* **17** 29–48.
- JÜRGENS, M., MEINERT, N., BENGIS, V., HÜLLERMEIER, E. and WAEGEMAN, W. (2024). Is Epistemic Uncertainty Faithfully Represented by Evidential Deep Learning Methods? Available at [arXiv:2402.09056](https://arxiv.org/abs/2402.09056).
- KAUR, R., JI, X., DUTTA, S., CAPRIO, M., YANG, Y., BERNARDIS, E., SOKOLSKY, O. and LEE, I. (2023). Using Semantic Information for Defining and Detecting OOD Inputs. Available at [arXiv:2302.11019](https://arxiv.org/abs/2302.11019).
- KENDALL, A. and GAL, Y. (2017). What uncertainties do we need in bayesian deep learning for computer vision? *Advances in neural information processing systems* **30**.
- KIM, J.-H., CHOO, W. and SONG, H. O. (2020). Puzzle Mix: Exploiting Saliency and Local Statistics for Optimal Mixup. In *Proceedings of the 37th International Conference on Machine Learning* (H. D. III and A. SINGH, eds.). *Proceedings of Machine Learning Research* **119** 5275–5285. PMLR.
- KRIZHEVSKY, A. (2012). Learning Multiple Layers of Features from Tiny Images. *University of Toronto*.
- KRIZHEVSKY, A., NAIR, V. and HINTON, G. (2009). CIFAR-10 (Canadian Institute For Advanced Research) Technical Report, CIFAR.
- LAMBROU, A., PAPADOPOULOS, H. and GAMMERMAN, A. (2010). Reliable confidence measures for medical diagnosis with evolutionary algorithms. *IEEE Transactions on Information Technology in Biomedicine* **15** 93–99.
- LE, Y. and YANG, X. (2015). Tiny imagenet visual recognition challenge. *CS 231N* **7** 3.
- LECUN, Y. and CORTES, C. (2005). The MNIST Database of Handwritten Digits. In *Proceedings of the IEEE Conference on Computer Vision and Pattern Recognition (CVPR)* 1–9. <https://doi.org/10.1109/CVPR.2005.177>
- LEVI, I. (1980). *The Enterprise of Knowledge*. London, UK : MIT Press.
- LIN, V., JANG, K. J., DUTTA, S., CAPRIO, M., SOKOLSKY, O. and LEE, I. (2023). Reversing Distribution Shifts using Reinforcement Learning. Available at [arXiv:2302.10341](https://arxiv.org/abs/2302.10341).
- MANCHINGAL, S. K. and CUZZOLIN, F. (2022). Epistemic Deep Learning. Available at [arxiv:2206.07609](https://arxiv.org/abs/2206.07609).
- MANCHINGAL, S. K., MUBASHAR, M., WANG, K., SHARIATMADAR, K. and CUZZOLIN, F. (2023). Random-Set Convolutional Neural Network (RS-CNN) for Epistemic Deep Learning. Available at [arxiv:2307.05772](https://arxiv.org/abs/2307.05772).
- MARINACCI, M. (1999). Limit laws for non-additive probabilities and their frequentist interpretation. *Journal of Economic Theory* **84** 145–195.
- MASSON, M.-H. and DENÈUX, T. (2008). ECM: An evidential version of the fuzzy c-means algorithm. *Pattern Recognition* **41** 1384–1397.
- NETZER, Y., WANG, T., COATES, A., BISSACCO, A., WU, B., NG, A. Y. et al. (2011). Reading digits in natural images with unsupervised feature learning. In *NIPS workshop on deep learning and unsupervised feature learning* **2011** 7. Granada, Spain.
- PANDEY, D. S. and YU, Q. (2023). Learn to Accumulate Evidence from All Training Samples: Theory and Practice. In *Proceedings of the 40th International Conference on Machine Learning* (A. KRAUSE, E. BRUNSKILL, K. CHO, B. ENGELHARDT, S. SABATO and J. SCARLETT, eds.). *Proceedings of Machine Learning Research* **202** 26963–26989. PMLR.
- PAWITAN, Y. (2001). *In All Likelihood: Statistical Modelling and Inference Using Likelihood*. Oxford University Press, Oxford.
- PREPARATA, F. P. and SHAMOS, M. I. (1985). *Computational Geometry: An Introduction*. Springer-Verlag, Berlin, Heidelberg.
- REN, Y., BAHAMOU, A. and GOLDFARB, D. (2022). Kronecker-factored Quasi-Newton Methods for Deep Learning. Available at [arXiv:2102.06737](https://arxiv.org/abs/2102.06737).
- REZENDE, D. and MOHAMED, S. (2015). Variational Inference with Normalizing Flows. In *Proceedings of the 32nd International Conference on Machine Learning* (F. BACH and D. BLEI, eds.). *Proceedings of Machine Learning Research* **37** 1530–1538. PMLR, Lille, France.

- SALE, Y., CAPRIO, M. and HÜLLERMEIER, E. (2023). Is the volume of a credal set a good measure for epistemic uncertainty? In *Proceedings of the Thirty-Ninth Conference on Uncertainty in Artificial Intelligence* (R. J. EVANS and I. SHPITSER, eds.). *Proceedings of Machine Learning Research* **216** 1795–1804. PMLR.
- SENIGE, R., BÖSNER, S., DEMBCZYŃSKI, K., HAASENRITTER, J., HIRSCH, O., DONNER-BANZHOF, N. and HÜLLERMEIER, E. (2014). Reliable Classification: Learning Classifiers That Distinguish Aleatoric and Epistemic Uncertainty. *Information Sciences* **255** 16–29.
- SHAFER, G. and VOVK, V. (2008). A Tutorial on Conformal Prediction. *Journal of Machine Learning Research* **9** 371–421.
- SHYAMALKUMAR, N. D. (2000). Likelihood Robustness. In *Robust Bayesian Analysis* (D. R. Insua and F. Ruggeri, eds.) 127–143. Springer New York, New York, NY.
- SMIEJA, M. and TABOR, J. (2012). Entropy of the Mixture of Sources and Entropy Dimension. *IEEE Transactions on Information Theory* **58** 2719–2728.
- SMITH, L. and GAL, Y. (2018). Understanding measures of uncertainty for adversarial example detection. *arXiv preprint arXiv:1803.08533*.
- ULMER, D. T., HARDMEIER, C. and FRELLSEN, J. (2023). Prior and Posterior Networks: A Survey on Evidential Deep Learning Methods For Uncertainty Estimation. *Transactions on Machine Learning Research*.
- VARSHNEY, K. R. (2016). Engineering safety in machine learning. In *2016 Information Theory and Applications Workshop (ITA)* 1–5. IEEE.
- VARSHNEY, K. R. and ALEMZADEH, H. (2017). On the safety of machine learning: Cyber-physical systems, decision sciences, and data products. *Big data* **5** 246–255.
- WALLEY, P. (1991). *Statistical Reasoning with Imprecise Probabilities*. *Monographs on Statistics and Applied Probability* **42**. London : Chapman and Hall.
- WALLEY, P. (1996). Inferences from Multinomial Data: Learning about a Bag of Marbles. *Journal of the Royal Statistical Society. Series B (Methodological)* **58** 3–57.
- XIAO, H., RASUL, K. and VOLLGRAF, R. (2017). Fashion-MNIST: a novel image dataset for benchmarking machine learning algorithms. *arXiv preprint arXiv:1708.07747*.
- YANG, F., WANG, H.-Z., MI, H., LIN, C.-D. and CAI, W.-W. (2009). Using random forest for reliable classification and cost-sensitive learning for medical diagnosis. *BMC bioinformatics* **10** 1–14.
- ZAFFALON, M. (2002). The naive credal classifier. *Journal of Statistical Planning and Inference* **105** 5–21. Imprecise Probability Models and their Applications. [https://doi.org/10.1016/S0378-3758\(01\)00201-4](https://doi.org/10.1016/S0378-3758(01)00201-4)
- ZAFFALON, M. and FAGIUOLI, E. (2003). Tree-Based Credal Networks for Classification. *Reliable Computing* **9** 487–509.

APPENDIX A: EPISTEMIC PROBABILITY

EU should not be confused with the concept of *epistemic probability* (de Finetti, 1974, 1975; Walley, 1991). In the subjective probability literature, epistemic probability can be captured by a single distribution. Its best definition can be found in (Walley, 1991, Sections 1.3.2 and 2.11.2). There, the author specifies how epistemic probabilities model logical or psychological degrees of partial belief of the agent. We remark, though, how de Finetti and Walley work with finitely additive probabilities, while in this paper we use countably additive probabilities.

APPENDIX B: FURTHER RELATED WORK

Robust classification via credal sets is a lively field. In (Corani, Antonucci and Zaffalon, 2012), the authors introduce credal classifiers (CCs), as a generalization of classifiers based on Bayesian networks. Unlike CCs, CDEC and IDEC do not require independence assumptions between non-descendant, non-parent variables. In addition, CDEC and IDEC avoid NP-hard complexity issues of searching for optimal structure in the space of Bayesian networks (Chickering, Heckerman and Meek, 2004). For a review of the state of the art concerning the distinction between EU and AU we refer to (Hüllermeier and Waegeman, 2021; Manchingal and Cuzzolin, 2022; Manchingal et al., 2023) and (Caprio et al., 2024a, Section 6 and Appendix O).

APPENDIX C: GENERAL OPERATIVE BOUNDS FOR EU AND TU

THEOREM C.1 (Bounds for Total and Epistemic Uncertainties). *Let \mathcal{P} be a finitely generated credal set, and let $ex\mathcal{P} = \{P_s^{ex}\}_{s=1}^S$ denote the set of its extreme elements.²¹ Let Δ^{S-1} denote the S -dimensional unit simplex,*

$$\Delta^{S-1} := \left\{ \beta = (\beta_1, \dots, \beta_S)^\top : \beta_s \geq 0 \text{ for all } s, \text{ and } \sum_s \beta_s = 1 \right\}.$$

Let $\underline{H}(P^{ex}) := \min_{P^{ex} \in ex\mathcal{P}} H(P^{ex})$ and $\overline{H}(P^{ex}) := \max_{P^{ex} \in ex\mathcal{P}} H(P^{ex})$. Let $TU(\mathcal{P})$, $AU(\mathcal{P})$, $EU(\mathcal{P})$ denote the total, aleatoric, and epistemic uncertainties associated with \mathcal{P} . By equation (4), we know that $TU(\mathcal{P}) = \overline{H}(P)$, $AU(\mathcal{P}) = \underline{H}(P)$, and $EU(\mathcal{P}) = \overline{H}(P) - \underline{H}(P)$. Let

$$l[TU(\mathcal{P})] := \max \left\{ \sup_{\beta \in \Delta^{S-1}} \sum_{s=1}^S \beta_s H(P_s^{ex}), \overline{H}(P^{ex}) \right\}.$$

Then,

$$(15) \quad TU(\mathcal{P}) \in \left[l[TU(\mathcal{P})], \sup_{\beta \in \Delta^{S-1}} \sum_{s=1}^S \beta_s H(P_s^{ex}) + \log_2(S) \right],$$

$$AU(\mathcal{P}) = \underline{H}(P^{ex}),$$

$$EU(\mathcal{P}) \in \left[\max \left\{ 0, l[TU(\mathcal{P})] - \underline{H}(P^{ex}) \right\}, \right.$$

$$(16) \quad \left. \sup_{\beta \in \Delta^{S-1}} \sum_{s=1}^S \beta_s H(P_s^{ex}) + \log_2(S) - \underline{H}(P^{ex}) \right].$$

²¹We assume without loss of generality that set \mathcal{P} has S many extreme elements.

APPENDIX D: GENERALIZED HARTLEY MEASURE

In (Bronevich and Rozenberg, 2021; Hüllermeier and Waegeman, 2021), the authors introduce the notion of *generalized Hartley measure* $GH(\mathcal{P})$ of set \mathcal{P} . Let the probabilities in \mathcal{P} be defined on a finite set $\mathcal{Y} = \{1, \dots, k\}$. Then,

$$(17) \quad GH(\mathcal{P}) := \sum_{A \in 2^{\mathcal{Y}}} \left[\log_2(|A|) \cdot \sum_{B \in 2^A} \left((-1)^{|A \setminus B|} \inf_{P \in \mathcal{P}} P(B) \right) \right],$$

where $2^{\mathcal{Y}}$ and 2^A denote the power sets of \mathcal{Y} and A , respectively, $|A|$ denotes the cardinality of set A , and $A \setminus B := A \cap B^c$. The uncertainties are given by

$$\underbrace{\overline{H}(P)}_{\text{total uncertainty TU}(\mathcal{P})} = \underbrace{[\overline{H}(P) - GH(\mathcal{P})]}_{\text{aleatoric uncertainty AU}(\mathcal{P})} + \underbrace{GH(\mathcal{P})}_{\text{epistemic uncertainty EU}(\mathcal{P})}.$$

Quantifying and disentangling AU and EU via the generalized Hartley measure enjoys desirable properties (Abellán and Klir, 2005; Hüllermeier and Waegeman, 2021; Jiroušek and Shenoy, 2018). Despite this, its definition (17) is such that using it in an applied setting becomes very difficult when $|\mathcal{Y}|$ is even moderate, say greater than 5 or 6. This is due to the sums, that are taken over the power sets, which make the computational cost become burdensome very fast. For this reason, in sections 3 and 4 we preferred to work with lower and upper entropy.

APPENDIX E: DIFFERENT TYPES OF AMBIGUITY AND DEGREE OF CONSERVATIVENESS OF OUR IHDR

In this section, we discuss a subtle difference between the procedures in sections 4 and 5, and we give a way of quantifying the degree of conservativeness of $IR_{\gamma}[\mathcal{I}(\ell, (1+d)\ell)]$, for a generic $d \geq 0$.

In Credal Deep Evidential Classification, presented in Algorithm 1, the agent faces *likelihood ambiguity*, that is, ambiguity around which correct likelihood to select for the analysis. This motivates them to specify different encoders and normalizing flows that, in turn, give different possible parameterizations for the Dirichlet posteriors. This ambiguity percolates through the whole procedure, and manifests itself in the posterior predictive set $\text{Conv}(\{\text{Cat}(\pi'_s)_{s=1}^S\})$. On the contrary, in Interval Deep Evidential Classification (IDEC), presented in Algorithm 2, the ambiguity is expressed by the agent directly on the posterior predictive distribution. We call it *predictive ambiguity*. This is done by assuming that the pmf \hat{p} of the true posterior predictive distribution \hat{P} belongs to $\mathcal{I}[\ell, (1+d)\ell]$.

From Definition 4.2, we have that $\overline{P}(Y \in IR_{\gamma}[\mathcal{I}(\ell, (1+d)\ell)]) = 1 - \gamma$. In turn, this implies that $\overline{P}(Y \in IR_{\gamma}[\mathcal{I}(\ell, (1+d)\ell)]) \geq 1 - \gamma$. The larger the distance between $\overline{P}(Y \in IR_{\gamma}[\mathcal{I}(\ell, (1+d)\ell)])$ and $1 - \gamma$, the more conservative the IHDR is. In (Coolen, 1992, Section 2), the author gives a way of quantifying this distance. We have that

$$(18) \quad \overline{P}(Y \in IR_{\gamma}[\mathcal{I}(\ell, (1+d)\ell)]) - (1 - \gamma) = \frac{\gamma(1 - \gamma)d(2 + d)}{(1 - \gamma)(1 + d)^2 + \gamma}.$$

The closer the value in (18) is to γ – that is, the closer $\overline{P}(Y \in IR_{\gamma}[\mathcal{I}(\ell, (1+d)\ell)])$ is to $1 - \gamma$ – the more conservative our IHDR is.

APPENDIX F: A k -DIMENSIONAL CLASSIFICATION PROBLEM WITH UNKNOWN k

Suppose that, in a classification problem, we do not know the correct number of classes. If that is the case, we can proceed in two ways. The first one is to specify a *mixture of finite*

mixtures prior, as explored e.g. in (Frühwirth-Schnatter, Malsiner-Walli and Grün, 2021). The second one is closer in spirit to the credal approach of section 4.

Let $Y_i \mid \pi, x_i \sim \text{Cat}(\pi)$ i.i.d., and assume that π is a K -dimensional vector, where K is the largest number of categories that we deem reasonable for the analysis at hand. As in section 3.1, this assumption allows to build a likelihood finitely generated credal set $\mathcal{P}_{\text{lik}} = \text{Conv}(\{\prod_{i=1}^{n_s^{\text{virt}}} p(y_i \mid \pi, x_i)\}_{s=1}^S)$. Consider then $M \geq 2$ Dirichlet priors, each parameterized by $\mathbf{1}_m$, a d_m -dimensional vector of all 1's, $d_m \equiv \dim(\mathbf{1}_m)$, $m \in \{1, \dots, M\}$. Of course, the dimension d_m of $\mathbf{1}_m$ must not exceed K , for all $m \in \{1, \dots, M\}$. Now extend every $\mathbf{1}_m$ as

$$\hat{\mathbf{1}}_m = \left(\mathbf{1}_{m,1}, \dots, \mathbf{1}_{m,d_m}, \underbrace{0, \dots, 0}_{K-d_m \text{ times}} \right)^\top,$$

and consider the “extended” Dirichlet priors $\text{Dir}(\hat{\mathbf{1}}_1), \dots, \text{Dir}(\hat{\mathbf{1}}_M)$. The prior FGCS, then, is $\mathcal{P}_{\text{prior}} = \text{Conv}(\{\text{Dir}(\hat{\mathbf{1}}_m)\}_{m=1}^M)$, and the posterior FGCS is

$$\mathcal{P}_{\text{post}} = \text{Conv}(\{\text{Dir}(\hat{\mathbf{1}}_m + c_s) : m \in \{1, \dots, M\}, s \in \{1, \dots, S\}\}),$$

where c_s is the K -dimensional vector such that $c_{s,j} = n_{s,j}^{\text{virt}}$, for all $s \in \{1, \dots, S\}$ and all $j \in \{1, \dots, K\}$, and $n_{s,j}^{\text{virt}}$ is the virtual number of observations introduced in section 3.1.

In turn, the predictive FGCS is

$$\mathcal{P}_{\text{pred}} = \text{Conv}(\{\text{Cat}(\hat{\pi}^{m,s}) : m \in \{1, \dots, M\}, s \in \{1, \dots, S\}\}),$$

where

$$\hat{\pi}_j^{m,s} = \frac{\hat{\mathbf{1}}_{m,j} + c_{s,j}}{\sum_{l=1}^K (\hat{\mathbf{1}}_{m,l} + c_{s,l})}, \quad j \in \{1, \dots, K\}.$$

The extreme elements $\text{ex}\mathcal{P}_{\text{pred}}$ of the predictive FGCS $\mathcal{P}_{\text{pred}}$ are obtained by running a convex hull algorithm like gift wrapping on $\{\hat{\pi}^{m,s} : m \in \{1, \dots, M\}, s \in \{1, \dots, S\}\}$ (Preparata and Shamos, 1985, Chapters 3, 4), similarly to what we did in section 4.2. Notice that the cardinality of $\text{ex}\mathcal{P}_{\text{pred}}$ is upper bounded by $M \cdot S$.

Then, the categories j whose upper predictive probability is small – that is, bounded by an arbitrarily small $\varepsilon > 0$ – are likely to be unnecessary and can be eliminated from the analysis.²² In formulas, if $\max_{j \in \{1, \dots, K\}} \text{ex} \hat{\pi}_j^{m,s} \leq \varepsilon$, then category j can be dropped from the study. Here, $\text{ex} \hat{\pi}^{m,s}$ denotes the parameters of the extreme elements $\text{ex}\mathcal{P}_{\text{pred}}$ of the predictive FGCS $\mathcal{P}_{\text{pred}}$. We can restrict our attention to the elements of $\{\text{ex} \hat{\pi}^{m,s}\}_{m,s}$ when computing the maximum as a result of (Caprio et al., 2024a, Proposition 2).

We conclude this section by noting how this method allows to build a model that addresses agnostic prior beliefs, ambiguity around the true data generating process, and uncertainty on the number of categories in the study. In the future, we plan to examine how the procedure proposed in this section compares to Nonparametric Predictive Inference (NPI, (Augustin et al., 2014, Chapter 7.6), (Hill, 1968)).

APPENDIX G: PROOFS

PROOF OF THEOREM 3.2. See the proof of Theorem C.1. □

PROOF OF THEOREM 4.3. Immediate from the superadditivity of lower probabilities (Cerrea-Vioglio, Maccheroni and Marinacci, 2015; Walley, 1991). □

²²Here, “small” has to be understood relatively to the values of the upper predictive probabilities of the other labels.

PROOF OF COROLLARY 5.2.1. Let $K = 2 \times |\mathcal{Y}|$. Then, consider K distributions Q_1, \dots, Q_K on \mathcal{Y} whose pmf's q_1, \dots, q_K are such that

1. $q_j(y_j) = \underline{P}(\{y_j\})$, and $q_j(y_s) \geq \underline{P}(\{y_s\})$, for all $j \in \{1, \dots, K/2\}$ and $y_s \in \mathcal{Y} \setminus \{y_j\}$,
2. $q_j(y_{j-K/2}) = \overline{P}(\{y_{j-K/2}\})$, and $q_j(y_s) \leq \overline{P}(\{y_s\})$, for all $j \in \{K/2 + 1, \dots, K\}$ and $y_s \in \mathcal{Y} \setminus \{y_{j-K/2}\}$.

Here the lower and upper probabilities of the elements of \mathcal{Y} are derived as in (8). Put then $\mathcal{P} = \text{Conv}(\{Q_r\}_{r=1}^K)$. According to Proposition 5.2, such a \mathcal{P} is a finitely generated credal set that corresponds to $\mathcal{I}(\ell, u)$. This concludes our proof. \square

PROOF OF THEOREM C.1. The proof is based on the following two results.

THEOREM G.1 (Bound for Upper Entropy and Value of Lower Entropy). *Let \mathcal{P} be a finitely generated credal set, and let $\text{ex}\mathcal{P} = \{P_s^{\text{ex}}\}_{s=1}^S$ denote the set of its extreme elements. Let Δ^{S-1} denote the S -dimensional unit simplex. Then,*

$$(19) \quad \underline{H}(P) = \underline{H}(P^{\text{ex}})$$

and

$$(20) \quad \sup_{\beta \in \Delta^{S-1}} \sum_{s=1}^S \beta_s H(P_s^{\text{ex}}) \leq \overline{H}(P) \leq \sup_{\beta \in \Delta^{S-1}} \left\{ \sum_{s=1}^S \beta_s H(P_s^{\text{ex}}) + \sum_{s=1}^S [-\beta_s \log_2(\beta_s)] \right\} \\ \leq \sup_{\beta \in \Delta^{S-1}} \sum_{s=1}^S \beta_s H(P_s^{\text{ex}}) + \log_2(S).$$

PROOF. We first show equation (19). Pick any $P' \in \mathcal{P}$. By the definition of \mathcal{P} , there exists a collection of non-negative reals $\{\beta_s\}_{s=1}^S$ such that $\sum_{s=1}^S \beta_s = 1$ and $\sum_{s=1}^S \beta_s P_s^{\text{ex}} = P'$. By the concavity of the entropy, we have that

$$H(P') = H\left(\sum_{s=1}^S \beta_s P_s^{\text{ex}}\right) \geq \sum_{s=1}^S \beta_s H(P_s^{\text{ex}}) \geq \sum_{s=1}^S \beta_s \underline{H}(P_s^{\text{ex}}) = \underline{H}(P^{\text{ex}}) := \min_{P^{\text{ex}} \in \text{ex}\mathcal{P}} H(P^{\text{ex}}).$$

Since P' was chosen arbitrarily from \mathcal{P} , and $\text{ex}\mathcal{P}$ is finite, this implies that

$$\inf_{P \in \mathcal{P}} H(P) =: \underline{H}(P) \geq \underline{H}(P^{\text{ex}}).$$

In addition, we have that, since $\text{ex}\mathcal{P} \subseteq \mathcal{P}$, $\underline{H}(P) \leq \underline{H}(P^{\text{ex}})$. Combining this with the above result, we obtain $\underline{H}(P) = \underline{H}(P^{\text{ex}})$. Next, we prove (20). In (Smieja and Tabor, 2012, Theorem III.1), the authors show that if a probability measure P can be written as $P = \sum_{s=1}^S \beta_s P_s^{\text{ex}}$, where $\beta = (\beta_1, \dots, \beta_S) \in \Delta^{S-1}$ and the elements of $\{P_s^{\text{ex}}\}_{s=1}^S$ are independent of one another, then

$$(21) \quad \sum_{s=1}^S \beta_s H(P_s^{\text{ex}}) \leq H\left(P = \sum_{s=1}^S \beta_s P_s^{\text{ex}}\right) \leq \sum_{s=1}^S \beta_s H(P_s^{\text{ex}}) + \sum_{s=1}^S [-\beta_s \log_2(\beta_s)] \\ \leq \sum_{s=1}^S \beta_s H(P_s^{\text{ex}}) + \log_2(S).$$

In addition, it is easy to see that $\overline{H}(P) := \sup_{P \in \mathcal{P}} H(P) = \sup_{\beta \in \Delta^{S-1}} H(\sum_{s=1}^S \beta_s P_s^{\text{ex}})$. In turn, taking the supremum over $\beta \in \Delta^{S-1}$ of the bounds for $H(P)$ in (21) gives us equation (20). \square

PROPOSITION G.2. (*Caprio et al., 2024a, Proposition 5*) Let \mathcal{P} be a finitely generated credal set, and let $ex\mathcal{P} = \{P_s^{ex}\}_{s=1}^S$ denote the set of its extreme elements. Let $\overline{H}(P^{ex}) := \max_{P^{ex} \in ex\mathcal{P}} H(P^{ex})$. Then,

$$(22) \quad \overline{H}(P) \geq \overline{H}(P^{ex}).$$

Then, the results presented in Theorem C.1 come immediately from Theorem G.1, Proposition G.2 and the definitions of TU(\mathcal{P}), AU(\mathcal{P}), and EU(\mathcal{P}) in (4). \square

APPENDIX H: ALGORITHMS

This section outlines the algorithms integral to the implementation of expected calibration error (ECE) (H.2) and OoD Detection: area under the receiver operating characteristic curve (AUROC) and area under the precision-recall curve (AUPRC) (H.1).

Algorithm 3 Expected Calibration Error (ECE)

Require: Predicted class-probabilities $p_i \in \mathbb{R}^K$ for all samples $i = 1, \dots, N$; true labels Y ; number of bins B .

Ensure: ECE value.

- 1: **Extract confidences and predictions:** $\text{conf}_i = \max_c p_i(c)$, $\hat{y}_i = \arg \max_c p_i(c)$.
 - 2: **Bin the samples:** Create B equal-width bins on $[0, 1]$ and assign each conf_i to a bin.
 - 3: **For each bin b :**
 - Let S_b be the set of samples in bin b .
 - Compute mean confidence $\widehat{\text{conf}}_b = \frac{1}{|S_b|} \sum_{i \in S_b} \text{conf}_i$.
 - Compute empirical accuracy $\widehat{\text{acc}}_b = \frac{1}{|S_b|} \sum_{i \in S_b} \mathbf{1}(\hat{y}_i = Y_i)$.
 - Compute bin weight $w_b = |S_b|/N$.
 - 4: **Compute ECE:** $\text{ECE} = \sum_{b=1}^B w_b \left| \widehat{\text{acc}}_b - \widehat{\text{conf}}_b \right|$.
-

H.1. Expected Calibration Error (ECE). Expected Calibration Error quantifies how closely a model's predicted confidences match the observed empirical accuracies. Given predictive probabilities $p_i \in \Delta^{K-1}$ for each sample i , we extract the predicted confidence

$$\text{conf}_i = \max_c p_i(c),$$

and the predicted class label

$$\hat{y}_i = \arg \max_c p_i(c).$$

The confidence values are partitioned into B equal-width bins on the interval $[0, 1]$. For each bin b , containing the set of indices S_b , we compute the average confidence

$$\widehat{\text{conf}}_b = \frac{1}{|S_b|} \sum_{i \in S_b} \text{conf}_i,$$

and the empirical accuracy

$$\widehat{\text{acc}}_b = \frac{1}{|S_b|} \sum_{i \in S_b} \mathbf{1}\{\hat{y}_i = y_i\}.$$

Each bin contributes proportionally to its size via the weight $w_b = |S_b|/N$, where N is the total number of samples.

The Expected Calibration Error is then

$$\text{ECE} = \sum_{b=1}^B w_b |\widehat{\text{acc}}_b - \widehat{\text{conf}}_b|.$$

This formulation matches the implementation used in our code: confidence is taken as the maximum predicted probability, bins are uniform on $[0, 1]$, and the ECE is computed using a fixed number of bins without temperature scaling or post-hoc smoothing. A lower ECE indicates better alignment between predicted and empirical correctness.

H.2. Algorithm for AUROC and AUPRC (OoD detection). To evaluate how well uncertainty distinguishes in-distribution (iD) from out-of-distribution (OoD) samples, we compute AUROC and AUPRC over uncertainty scores. For a given uncertainty measure $u(x)$ – aleatoric (AU), epistemic (EU), total uncertainty (TU), or confidence – we assign OoD samples as positives and iD samples as negatives. Since confidence is a decreasing measure of uncertainty, we convert it into an uncertainty score by negating the maximum predictive probability,

$$u(x) = -\max_c p(c | x).$$

Let $\{u_{\text{iD}}\}$ and $\{u_{\text{OoD}}\}$ denote the uncertainty scores for iD and OoD samples. We concatenate these into a single vector and create binary labels

$$y_i = \begin{cases} 0, & \text{iD sample,} \\ 1, & \text{OoD sample.} \end{cases}$$

The Receiver Operating Characteristic (ROC) curve is then computed from the pairs (TPR, FPR) obtained by thresholding the uncertainty score at all possible levels. The area under this curve defines the AUROC:

$$\text{AUROC} = \int_0^1 \text{TPR}(t) d\text{FPR}(t),$$

which we compute numerically via `roc_auc_score`.

Similarly, the Precision-Recall curve is computed from the pairs (Precision, Recall) evaluated at each threshold, and the area under this curve defines the AUPRC:

$$\text{AUPRC} = \int_0^1 \text{Precision}(r) d\text{Recall}(r),$$

computed using `average_precision_score`.

This procedure exactly matches the implementation in our evaluation code: uncertainty values for iD and OoD are concatenated, binary labels are created, and AUROC/AUPRC are computed directly from these scores without additional calibration or smoothing.

APPENDIX I: ADDITIONAL EXPERIMENTS AND RESULTS

I.1. Training details. All Posterior Network models are trained using three random seeds ($\{322, 365, 382\}$), and we evaluate every trained model without any form of sub-sampling. The following hyperparameters are fixed across all datasets and architectures unless otherwise stated. All Posterior Networks are implemented with hidden-layer widths of $([64, 64, 64])$, a latent dimensionality of 6, a kernel size of 5 for convolutional encoders, and six radial-flow components per class. Training is performed for a maximum of 200 epochs using the Adam optimizer with a learning rate of 10^{-4} , batch size of 128, and no learning-rate

Algorithm 4 Computation of AUROC and AUPRC for OoD detection

Require: Uncertainty scores for in-distribution samples unc_{iD} , uncertainty scores for OoD samples unc_{OoD} . (For confidence, the uncertainty is $-\max p(c | x)$.)

Ensure: AUROC and AUPRC.

- 1: Concatenate uncertainty scores: $u = [\text{unc}_{\text{iD}}, \text{unc}_{\text{OoD}}]$.
 - 2: Create binary labels: $y = [0, \dots, 0, 1, \dots, 1]$ ($0 = \text{iD}$, $1 = \text{OoD}$).
 - 3: Compute ROC curve via $(\text{fpr}, \text{tpr}, \tau) = \text{roc_curve}(y, u)$.
 - 4: Compute AUROC via $\text{AUROC} = \text{roc_auc_score}(y, u)$.
 - 5: Compute precision-recall curve via $(\text{precision}, \text{recall}, \tau_{\text{PR}}) = \text{precision_recall_curve}(y, u)$.
 - 6: Compute AUPRC via $\text{AUPRC} = \text{average_precision_score}(y, u)$.
-

scheduling. The evidential loss includes a Dirichlet entropy regularizer with weight 10^{-6} . Early stopping is applied with a validation-check frequency of two epochs and a patience threshold of five such checks. All models are trained in full FP32 precision due to the numerical sensitivity of the normalizing-flow layers.

The preprocessing pipeline used for all datasets follows exactly the backbone-aware normalization described in the main paper. MNIST, KMNIST and FashionMNIST each provide 60,000 training images and 10,000 test images after preprocessing; CIFAR-10 and CIFAR-100 provide 50,000 training and 10,000 test images; SVHN contributes 26,032 test images; Intel Image contains 3,000 test images; and TinyImageNet provides 10,000 validation images which are used exclusively as out-of-distribution inputs. All experiments are conducted without augmentations of any kind.

Each backbone-dataset pair is trained independently for the three seed values $\{322, 365, 382\}$. These seeds affect both the encoder initialization and the initial parameters of the flow components, thereby producing distinct Dirichlet families and inducing the diversity required for credal-set formation. In all cases, the same hyperparameters are used for every backbone to ensure comparability across architectures.

Table 5 summarizes the complete set of training parameters.

In addition to the main experiments, we conduct an ablation study (section 6.6) on the effect of ensemble size for CDEC. For this study, we train Posterior Networks using ten random seeds: 322, 365, 382, 410, 411, 412, 413, 414, 415, 416. From these ten trained models we construct ensembles of sizes $S \in \{1, 3, 5, 7, 10\}$, always using the first S seeds in their natural ordering. Each ensemble is evaluated using the exact convex-extreme-point procedure of CDEC, and we record the resulting IHDR sizes, IHDR coverage, aleatoric uncertainty, epistemic uncertainty, and total uncertainty. This ablation isolates the contribution of ensemble diversity to the geometry and informativeness of the learned credal sets. All experiments are run on NVIDIA A100 GPUs (80GB). Training a single Posterior Network requires between 15 and 90 minutes depending on the backbone.

I.2. Adaptability to different backbone architectures. This section reports the extended experimental results for all four backbone architectures considered in our study: a lightweight convolutional network (Conv), VGG16, ResNet18, and ResNet50.

I.2.1. Predictive Performance across all backbones. Tables 6, 7 and 8 report the full predictive performance of PostNet, PostNet-3, CDEC-3 and IDEC across all datasets and the three remaining backbone architectures (Conv, VGG16 and ResNet18). These results complement the ResNet-50 evaluation presented in Table 2 and confirm that the empirical trends reported in section 6 hold *consistently* across architectural families of varying depth and capacity.

Across nearly all dataset-backbone combinations, CDEC-3 yields the best or near-best accuracy and Brier score. The improvement is most pronounced on higher-complexity datasets

TABLE 5
Training Hyperparameters and Model Configuration

Parameter	Value
Architectures	Conv, VGG16, ResNet18, ResNet50
Posterior Network Hidden Layers	[64, 64, 64]
Latent Dimension (PN)	6
Normalizing Flow Type	Radial flow
Flow Components	6
Output Distribution	Dirichlet (predictive mean $p = \alpha/\alpha_0$)
Loss Function	UCE (Evidential Cross-Entropy)
Optimizer	Adam
Learning Rate	1×10^{-4}
Batch Size	128
Epochs	200 (with early stopping)
Early-Stopping Frequency	every 2 epochs
Patience	5
Regularisation (regr)	1×10^{-6}
Confidence Target	$1 - \gamma = 0.95$
Seeds per Backbone	{322, 365, 382}
Training Hardware	NVIDIA A100 80GB
Dataset Sizes	MNIST: 60,000 train / 10,000 test CIFAR-10: 50,000 train / 10,000 test CIFAR-100: 50,000 train / 10,000 test SVHN: 26,032 test Intel Image: 3,000 test KMNIST: 10,000 test FashionMNIST: 10,000 test TinyImageNet: 10,000 validation
Input Resolution (conv)	MNIST: 28×28 ; CIFAR: 32×32
Input Resolution (VGG/ResNet)	upsampled to 32×32 (RGB)
Data Augmentation	None

Model	In-distribution (MNIST)						OoD Detection Performance				
	Prediction Performance			Uncertainty Estimation			F-MNIST		K-MNIST		
	Acc (↑)	Brier (↓)	ECE (↓)	AU mean (↓)	EU mean (↓)	TU mean (↓)	AUROC (↑)	AUPRC (↑)	AUROC (↑)	AUPRC (↑)	
Conv	PostNet	99.02	0.0153	0.0026	0.4159	0.0000	0.4159	98.80	98.57	97.00	96.85
	PostNet-3	99.41	0.0100	0.0032	0.1297	1.4448	1.5745	99.40	98.79	99.02	98.44
	CDEC-3	99.43	0.0162	0.0134	0.0040	1.1469	1.1509	99.63	99.58	99.27	99.17
	IDEC	99.31	0.0109	0.0038	0.0050	9.5331e6	9.5331e6	99.27	98.79	98.55	98.30
VGG16	PostNet	97.63	0.0310	0.0065	0.7278	0.0000	0.7278	94.87	90.25	94.94	90.15
	PostNet-3	99.54	0.0097	0.0076	0.0285	1.8015	1.8300	97.76	96.97	97.18	96.08
	CDEC-3	99.54	0.0279	0.0252	0.0009	1.1597	1.1606	98.15	98.11	97.77	97.61
	IDEC	99.47	0.0096	0.0044	0.0018	1.5275e6	1.5275e6	99.07	98.69	98.64	98.46
ResNet18	PostNet	97.96	0.0267	0.0044	0.8759	0.0000	0.8759	97.06	93.54	96.32	91.26
	PostNet-3	99.32	0.0098	0.0072	0.0906	1.8864	1.9769	98.84	98.36	97.73	96.45
	CDEC-3	99.44	0.0264	0.0251	0.0027	1.1739	1.1766	99.26	99.14	98.55	98.37
	IDEC	99.42	0.0102	0.0041	0.0042	1.0893e6	1.0893e6	97.91	97.64	98.68	98.43
ResNet50	PostNet	92.24	0.0794	0.0102	2.3888	0.0000	2.3888	90.74	80.27	90.44	79.83
	PostNet-3	99.04	0.0388	0.0311	0.3767	3.1372	3.5139	95.12	93.47	95.59	94.58
	CDEC-3	99.42	0.0914	0.0986	0.0033	1.3575	1.3608	97.15	96.87	96.97	96.86
	IDEC	99.31	0.0216	0.0054	0.0162	4.2985e15	4.2985e15	96.61	92.63	93.85	90.40

TABLE 6
Evaluation of predictive performance, uncertainty decomposition, and OoD detection for all models on MNIST on all backbones.

(CIFAR-10, CIFAR-100), where model uncertainty is substantial and the advantage of credal reasoning becomes more visible. By restricting aggregation to only the *extreme points* of the ensemble’s posterior predictive set, CDEC avoids the entropy inflation induced by uniformly averaging all ensemble members. This produces sharper yet well-regularized predictions, re-

Model		In-distribution (CIFAR-10)						OoD Detection Performance			
		Prediction Performance			Uncertainty Estimation			SVHN		Intel	
		Acc (↑)	Brier (↓)	ECE (↓)	AU mean (↓)	EU mean (↓)	TU mean (↓)	AUROC (↑)	AUPRC (↑)	AUROC (↑)	AUPRC (↑)
Conv	PostNet	78.48	0.3111	0.0656	5.9585	0.0000	5.9585	77.24	86.05	67.74	38.46
	PostNet-3	82.17	0.2441	0.0280	5.0453	2.7905	7.8358	71.12	79.98	71.42	36.73
	CDEC-3	82.58	0.3345	0.1814	0.2165	1.6199	1.8364	77.31	86.27	72.85	42.41
	IDEC	79.51	0.2060	0.0742	0.1875	709.4864	709.6740	78.71	86.64	69.25	37.60
VGG16	PostNet	68.78	0.4887	0.1822	5.3438	0.0000	5.3438	74.21	85.71	67.19	35.03
	PostNet-3	77.42	0.3319	0.0495	3.7782	2.8797	6.6578	63.16	75.88	69.22	34.30
	CDEC-3	77.57	0.4828	0.0242	0.0916	1.7217	1.8133	76.09	87.46	76.59	47.21
	IDEC	73.87	0.4217	0.1653	0.1397	1.1989e17	1.1989e17	74.93	86.27	75.99	54.30
ResNet18	PostNet	65.45	0.5232	0.1773	6.8539	0.0000	6.8539	84.65	92.77	61.71	30.85
	PostNet-3	78.89	0.3105	0.0430	4.4983	3.6214	8.1197	72.24	81.20	65.17	29.59
	CDEC-3	78.11	0.4821	0.2708	0.1209	1.8549	1.9758	80.10	88.49	69.49	36.80
	IDEC	75.70	0.3854	0.1368	0.1598	6.2678e16	6.2678e16	70.24	81.46	69.10	36.87
ResNet50	PostNet	81.52	0.2868	0.0906	4.0245	0.0000	4.0245	74.96	84.52	68.74	36.57
	PostNet-3	84.12	0.1988	0.0369	3.2563	2.36	5.62	75.17	83.66	73.60	38.69
	CDEC-3	86.44	0.1180	0.1865	0.0776	1.6244	1.7019	78.04	86.94	74.98	43.30
	IDEC	82.88	0.2656	0.0805	0.1291	4.3278e16	4.3278e16	75.04	84.41	70.17	36.52

TABLE 7

Evaluation of predictive performance, uncertainty decomposition, and OoD detection for all models on CIFAR-10 on all backbones.

		In-distribution (CIFAR-100)						OoD Detection Performance	
Model		Prediction Performance			Uncertainty Estimation			TinyImageNet	
		Acc (↑)	Brier (↓)	ECE (↓)	AU mean (↓)	EU mean (↓)	TU mean (↓)	AUROC (↑)	AUPRC (↑)
Conv	PostNet	35.18	0.7879	0.3555	3.1080	0.0000	3.1080	61.05	57.87
	PostNet-3	40.71	0.7143	0.0778	2.5875	2.0299	4.6175	63.65	59.33
	CDEC-3	42.70	0.8157	0.0235	1.7862	2.2833	4.0695	65.20	61.36
	IDEC	35.93	0.7827	0.0737	0.6986	1.7652	2.4638	61.98	58.82
VGG16	PostNet	23.73	0.9328	0.2133	2.8901	0.0000	2.8901	57.45	54.74
	PostNet-3	28.87	0.8019	0.2754	2.0763	2.7233	4.7996	59.18	55.14
	CDEC-3	31.99	0.9011	0.1916	1.5068	2.5829	4.0897	62.42	58.98
	IDEC	25.49	0.9369	0.2233	0.6585	0.2299	0.8884	57.77	55.44
ResNet18	PostNet	23.15	0.9404	0.2133	2.9619	0.0000	2.9619	56.09	52.93
	PostNet-3	30.82	0.8053	0.0698	1.9774	3.3567	5.3341	58.99	55.39
	CDEC-3	31.63	0.9009	0.0514	1.6664	2.5053	4.1717	62.25	58.70
	IDEC	25.43	0.9312	0.2262	0.6628	1.3397	2.0025	57.98	55.11
ResNet50	PostNet	53.93	0.7281	0.2868	0.9391	0.0000	0.9391	65.84	62.18
	PostNet-3	59.91	0.5182	0.0572	0.6989	1.7059	2.4048	67.01	60.05
	CDEC-3	62.84	0.4683	0.2618	0.1809	1.4482	1.6291	72.95	68.54
	IDEC	58.29	0.6978	0.2595	0.2693	11203.7291	11203.9984	65.75	60.45

TABLE 8

Evaluation of predictive performance, uncertainty decomposition, and OoD detection for all models on CIFAR-100 on all backbones.

ducing both miscalibration and probability mass spread, directly reflecting the theoretical properties of lower-envelope decision making. PostNet-3, by contrast, averages all ensemble members regardless of informativeness. This uniform mixture is known to attenuate decisive predictions when some members are high-entropy, leading to reduced sharpness and systematically higher Brier scores. The single-model PostNet variant performs worse still, as it lacks epistemic diversity and therefore cannot regularize miscalibrated outputs.

IDEC displays mixed behaviour across backbones. On simpler problems (MNIST), IDEC exhibits excellent calibration, frequently achieving the lowest ECE among all methods, due to its interval-corrected uncertainty representation. However, for more complex datasets such as CIFAR-100, enforcing global marginal coverage through the inflation parameter d^* may require substantial widening of the predictive intervals, yielding flatter class distributions and increasing Brier error. This effect becomes stronger for deeper backbones, whose sharper latent representations amplify the influence of interval inflation.

I.2.2. Uncertainty Estimation. Figures 3, 4 and 5 provide the full AU/EU/TU uncertainty distributions for all models and datasets. Each figure shows KDE estimates of in-distribution (iD) and OoD uncertainty under PostNet, PostNet-3, CDEC-3 and IDEC.

PostNet and PostNet-3 concentrate AU around small values while producing broad, diffuse epistemic distributions. For PostNet-3, this behaviour reflects disagreement within the ensemble and results in moderate EU separation between iD and OoD samples. However, TU remains strongly correlated with AU and fails to cleanly distinguish distributional shift.

CDEC-3 produces tightly concentrated AU (sharp minima of extreme-point entropy), with EU reflecting only the *credible* disagreement across extreme predictions. The resulting TU distributions demonstrate: (i) low variance on iD data, (ii) a clean upward shift on OoD data, and (iii) reduced tail-mass relative to PostNet ensembles. This confirms that the credal-extreme-point decomposition removes artificial epistemic variance and captures only genuine ambiguity.

As expected from the variance-based inflation model, IDEC shows: (i) near-identical AU distributions to PostNet (since AU corresponds to the categorical variance), (ii) very large EU terms when class probabilities are diffuse (e.g. CIFAR-100), due to the $(1 + d^*)^2$ scaling, and (iii) TU dominated almost entirely by epistemic contributions. The extreme EU/TU values observed on CIFAR-100 reflect the high-dimensional simplex geometry: even moderate uncertainty across 100 classes produces large categorical variance, and thus large inflated epistemic components.

CDEC propagates *discrete geometric uncertainty* from a credal set, yielding bounded and interpretable uncertainty profiles, whereas IDEC propagates *interval-inflated variance*, which can grow rapidly in high-class problems but remains meaningful as a conservative uncertainty certificate.

I.2.3. Out-of-distribution (OoD) Detection. Table 9 provides the full OoD detection metrics for all datasets (MNIST, CIFAR-10, CIFAR-100), all OoD shifts (F-MNIST, K-MNIST, SVHN, Intel, TinyImageNet), and all architectures (Conv, VGG16, ResNet18, ResNet50). Each uncertainty measure is evaluated separately (AU, EU, TU, conf) using AUROC and AUPRC.

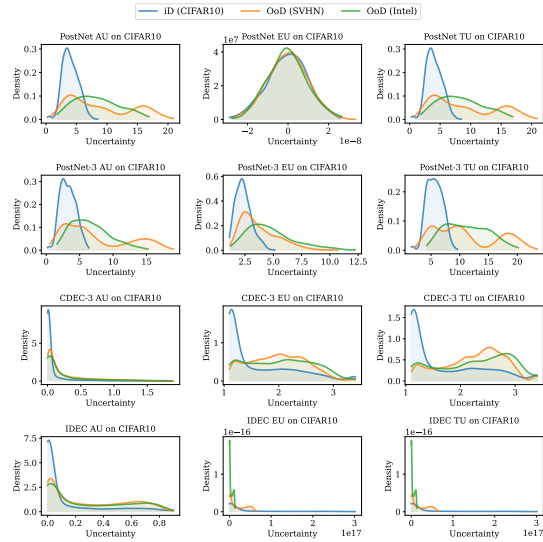


FIG 3. CIFAR-10 uncertainty distributions for PostNet, PostNet-3, CDEC-3 and IDEC.

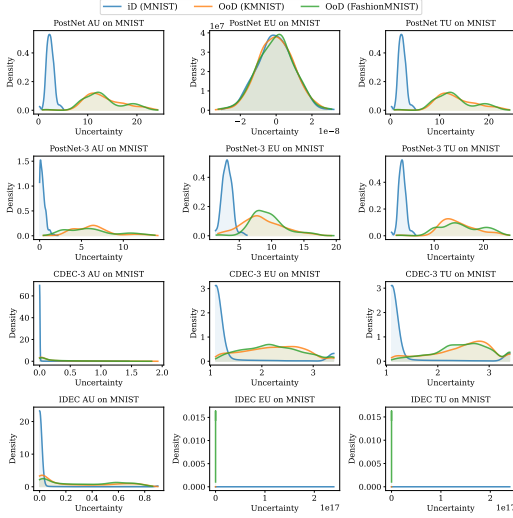


FIG 4. MNIST uncertainty distributions for PostNet, PostNet-3, CDEC and IDEC.

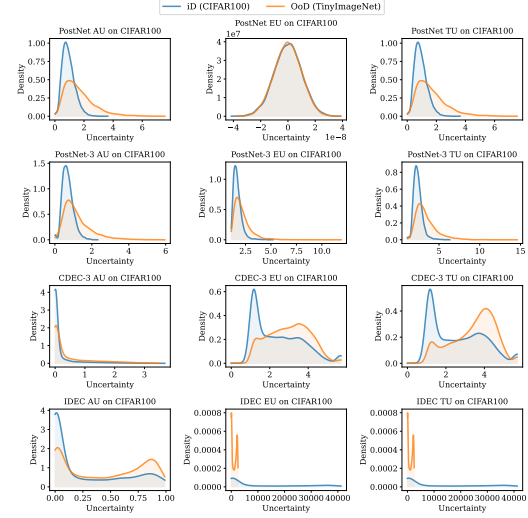


FIG 5. CIFAR-100 uncertainty distributions for PostNet, PostNet-3, CDEC and IDEC.

The results reinforce the conclusions from section 6.4: (i) CDEC-3 provides the strongest EU and TU-based separation across all architectures and all datasets. (ii) PostNet-3 improves over PostNet, but typically remains overconfident, especially on more complex datasets such as CIFAR-100. (iii) IDEC succeeds when the interval inflation parameter d^* remains moderate (MNIST, CIFAR-10). On CIFAR-100, however, required inflation becomes very large, flattening predictive distributions and diminishing contrast between iD and OoD.

Figure 6 illustrates how both CDEC and IDEC separate iD and OoD data in terms of their uncertainty profiles. Across MNIST, CIFAR-10, and CIFAR-100, the iD curves (solid lines) for AU, EU, and TU remain tightly concentrated near low uncertainty, whereas the OoD curves (dashed lines) shift rightward and become broader, indicating higher and more dispersed uncertainty under distribution shift.

For CDEC, this behavior is most pronounced, with iD densities exhibiting sharp peaks and OoD curves showing clear rightward drift. IDEC shows the same qualitative trend but with heavier-tailed densities, particularly on CIFAR-100. Overall, the KDE plots confirm that both CDEC and IDEC assign higher uncertainty to OoD samples, but CDEC produces the most compact iD distributions, resulting in clearer separation.

I.2.4. Additional IHDR analysis and visualizations. In this appendix, we provide extended empirical analysis of the Imprecise Highest Density Region (IHDR) beyond what is

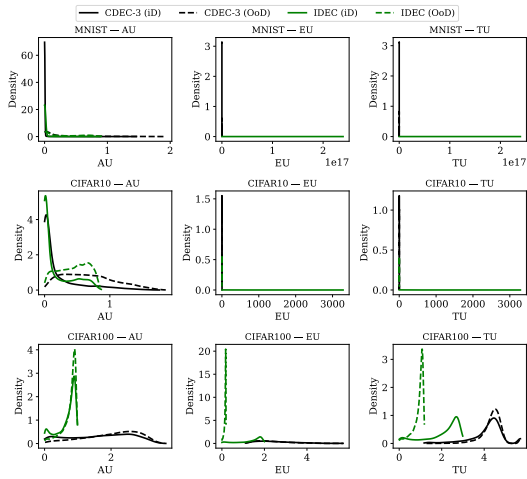


FIG 6. Uncertainty distributions (AU, EU, TU) for CDEC and IDEC evaluated on MNIST, CIFAR-10, and CIFAR-100. Each subplot compares in-distribution (iD, solid curves) and out-of-distribution (OoD, dashed curves) samples.

iD	Dataset	Model	OoD Detection Performance (%)							
			AUROC (AU)	AUPRC (AU)	AUROC (EU)	AUPRC (EU)	AUROC (TU)	AUPRC (TU)	AUROC (conf)	AUPRC (conf)
MNIST	F-MNIST	PostNet	99.84	99.87	50.00	50.00	99.84	99.87	90.74	80.27
		PostNet-3	98.66	98.41	97.27	92.19	97.83	94.41	95.12	93.47
		CDEC-3	99.99	99.99	98.56	98.97	99.89	99.90	97.15	96.87
		IDEC	97.92	97.68	33.95	39.68	33.95	39.68	96.61	92.63
	K-MNIST	PostNet	99.76	99.83	50.00	50.00	99.76	99.83	90.44	79.83
		PostNet-3	99.04	98.96	96.29	90.30	97.21	92.05	95.59	94.68
		CDEC-3	99.99	99.99	99.15	99.33	99.93	99.94	96.97	96.86
		IDEC	98.69	98.44	18.52	34.21	18.53	34.21	93.85	90.40
CIFAR-10	SVHN	PostNet	99.75	99.92	50.00	72.08	99.75	99.92	74.96	84.53
		PostNet-3	76.44	86.81	76.44	86.27	82.21	90.68	75.17	83.66
		CDEC-3	66.54	87.61	99.85	99.95	99.73	99.92	78.04	86.94
		IDEC	70.21	81.39	47.78	66.64	47.78	66.64	75.04	84.40
	Intel	PostNet	66.39	60.44	50.00	23.30	66.39	60.44	68.74	36.57
		PostNet-3	69.57	37.81	63.81	29.39	67.53	33.86	73.61	38.70
		CDEC-3	76.37	68.38	66.47	52.98	80.55	74.59	74.99	43.30
		IDEC	69.15	37.19	88.86	79.84	88.86	79.84	70.17	36.52
CIFAR-100	TinyImageNet	PostNet	73.85	78.54	50.00	50.00	73.85	78.54	65.84	62.18
		PostNet-3	68.10	65.52	65.08	58.24	68.49	61.41	67.01	60.05
		CDEC-3	72.49	77.21	70.02	72.23	77.09	80.15	72.95	68.54
		IDEC	65.89	60.67	37.12	40.20	37.12	40.20	65.75	60.45

TABLE 9

Full OoD detection performance (AUROC/AUPRC for AU, EU, TU, conf) across all datasets, OoD shifts, and backbones.

presented in section 6.5. IHDRs give a concrete, interpretable representation of the imprecision captured by a model’s posterior credal set, and therefore provide a useful diagnostic for understanding how uncertainty behaves under different data conditions.

IHDR size and coverage across datasets. Figure 7 displays the full distribution of IHDR cardinalities together with the mean coverage achieved by CDEC-3 and IDEC on MNIST, CIFAR-10, and CIFAR-100. Across all datasets, CDEC-3 yields extremely compact IHDRs on in-distribution samples (size ≈ 1 on MNIST, and typically < 7 on CIFAR-10), while maintaining nearly perfect coverage. IDEC, in contrast, produces broader IHDRs, especially on CIFAR-100 where the distribution spans dozens of classes. These results mirror the credal set statistics reported in the main text and highlight the structural differences between the two approaches: CDEC-3 concentrates probability mass onto small, highly specific hypothesis sets, whereas IDEC distributes mass across larger and more diffuse sets.

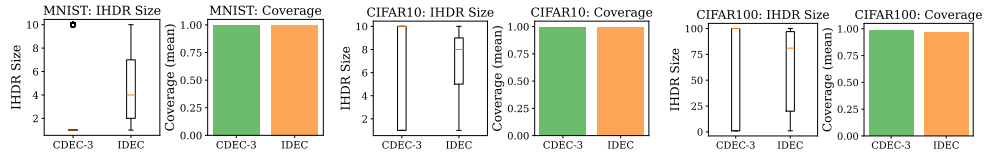


FIG 7. *IHDR size distributions and mean coverage on iD data. CDEC-3 consistently forms compact IHDRs with near-perfect coverage, whereas IDEC produces larger and more variable sets, especially on CIFAR-100.*

iD-OoD shift in IHDR size. Table 10 reports the mean IHDR size on iD data and compares it with the corresponding IHDR size on one or more OoD datasets. CDEC-3 consistently expands its IHDR under distribution shift (e.g. +7.3 and +7.5 on MNIST, +3.4—+3.8 on CIFAR-10, and a substantial +23.0 on CIFAR-100), providing a clear and monotonic signal of unfamiliarity. IDEC follows the same qualitative pattern, but with smaller shifts and occasional contractions (e.g. CIFAR-10—SVHN), suggesting that it is more sensitive to the backbone’s representation. These metrics confirm that CDEC-3 offers the most robust and interpretable distinction between iD and OoD samples in credal space.

Qualitative examples. Figure 8 provides qualitative illustrations of IHDRs for randomly selected test samples. On MNIST, CDEC-3 typically returns singleton or size-2 sets contain-

TABLE 10
iD vs OoD IHDR set size. iD size is the mean IHDR cardinality on in-distribution samples, OoD size is computed per OoD dataset, and Δ denotes the shift.

Dataset (iD)	Model	IHDR Size (iD) (\downarrow)	Dataset (OoD)	IHDR Size (OoD) (\uparrow)	Δ
MNIST	CDEC	2.28	KMNIST	9.56	+7.28
			F-MNIST	9.75	+7.48
	IDEC	4.55	KMNIST	7.97	+3.42
			F-MNIST	7.72	+3.18
CIFAR10	CDEC	5.34	SVHN	9.16	+3.81
			Intel	8.73	+3.39
	IDEC	6.76	SVHN	5.10	-1.66
			Intel	7.14	+0.38
CIFAR100	CDEC	73.03	TinyImageNet	96.05	+23.02
	IDEC	61.51	TinyImageNet	70.12	+8.61

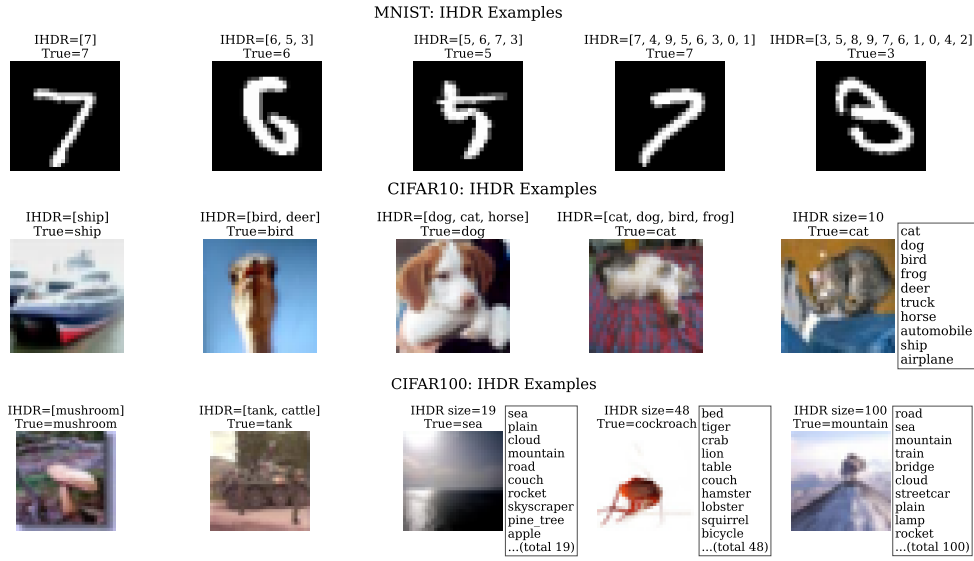


FIG 8. **IHDR examples.** For each dataset, we display randomly selected test samples and their corresponding IHDR sets. CDEC-3 typically returns compact and semantically coherent sets, whereas IDEC may return larger or more diffuse sets, especially on fine-grained tasks such as CIFAR-100.

ing the correct digit, whereas IDEC often includes multiple neighboring digits. On CIFAR-10, CDEC-3 yields small, semantically coherent IHDRs (e.g. *dog–cat–horse*), while IDEC occasionally includes a broader set of plausible classes. On CIFAR-100, where fine-grained distinctions are harder, both models produce larger IHDRs, but CDEC-3 remains comparatively compact, whereas IDEC may return dozens of classes. These examples demonstrate that IHDRs provide transparent, human-interpretable indicators of model uncertainty, especially under class overlap or ambiguous visual appearance.

Therefore, CDEC-3 induces a stable, interpretable credal representation whose iD and OoD behavior remains consistent across datasets and backbones: (i) CDEC-3 consistently forms compact and high-coverage IHDRs on iD data, (ii) both models expand IHDR size under distribution shift, but CDEC-3 does so more reliably, and (iii) qualitative IHDRs reveal structured, semantically meaningful sets that align with visual ambiguity.